January 2014

Novel Sustainable Structural Materials By Using Benign Waste Materials

M Faisal Riyad

NOVEL SUSTAINABLE STRUCTURAL MATERIALS BY USING BENIGN WASTE MATERIALS

by

M Faisal Riyad

Bachelor of Science, Khulna University of Engineering & Technology, Khulna, 2009

A Thesis

Submitted to the Graduate Faculty

of the

University of North Dakota

in partial fulfillment of the requirements

for the degree of

Master of Science

Grand Forks, North Dakota
December
2014

This thesis, submitted by M Faisal Riyad in partial fulfillment of the requirements for the Degree of Master of Science from the University of North Dakota, has been read by the Faculty Advisory Committee under whom the work has been done and is hereby approved.

_____
Chairperson (Dr. Surojit Gupta)

_____
Dr. Matthew Cavalli

_____
Dr. Bishu Bandyopadhyay

This thesis meets the standards for appearance, conforms to the style and format requirements of the Graduate School of the University of North Dakota, and is hereby approved.

_____
Wayne Swisher
Dean of the Graduate School

_____
Date

PERMISSION

Title Novel Sustainable Structural Materials By Using Benign Waste Materials

Department Mechanical Engineering

Degree Master of Science

In presenting this thesis in fulfillment of the requirements for a graduate degree from the University of North Dakota, I agree that the library of this University shall make it freely available for inspection. I further agree that permission for extensive copying for scholarly purposes may be granted by the professor who supervised my thesis work or, in his absence, by the chairperson of the department or the dean of the Graduate School. It is understood that any copying or publication or other use of this thesis or part thereof for financial gain shall not be allowed without my written permission. It is also understood that due recognition shall be given to me and to the University of North Dakota in any scholarly use which may be made of any material in my thesis.

Signature M Faisal Riyad

Date 12/09/2014

CONTENTS

LIST OF FIGURES

LIST OF TABLES

Table Page

ACKNOWLEDGEMENTS

All praises and thanks to the Almighty, the most beneficent and most merciful, who gave me abilities and helped me to complete this thesis.

I would like to express my gratitude to my supervisor, Dr. Surojit Gupta for his support and encouragement which has made the successful completion of this work. Throughout my work he tried to help me with my understanding, concepts and most of all to improve my research skills as well. I am also grateful to my thesis committee members, Dr. Matthew Cavalli and Dr. Bishu Bandyopadhyay for their invaluable suggestions and guidance. I also would like to acknowledge the Department of Mechanical Engineering, UND for giving me financial supports throughout my graduate studies.

In closing, I am very grateful to my family for their love, support and patience in my absence.

ABSTRACT

We propose a Green Cement Paradigm (GCPa) for fabricating environmentally friendly cementitious materials. By using GCPa, we report for the first time, the usage of Class C Fly Ash as a sole source of cementitous phase without any activation by alkali. During this study, Class C Fly Ash, and its composites with sand were fabricated at different compaction stresses by maintaining a low w/c (w-water, c-cement) ratio of 0.17-0.24 in the compacts. The porosity and the number of days for curing played a significant role in the evolution of compressive strength. The experimental results indicate that the curing for 28 days is the optimum time required for strength development. For example, the Class C Fly Ash samples cold pressed at ~86 MPa and cured for 28 days showed a compressive strength of ~29.5 MPa. The effect of additional $Ca(OH)_2$, high temperature curing and carbonation on the compressive strength development of the class C FA samples is reported. SEM, EDS, TGA/DSC and XRD investigations were employed to explain the obtained results. The possibility of fabricating lignin based polymer composites was investigated. The mechanical properties of the composites were reported in terms of yield strength and flexural strength.

CHAPTER I
INTRODUCTION

Fly ash (FA) is the principal by-product during the combustion of pulverized coal in thermal power plants [1, 2]. Coal combustion is an important mean to raise electricity in several countries. For example, eight countries use more than 100 Mt coal/year, with China using >2.5 Gt/year and the United States using over 0.73 Gt/year [3]. According to the 2009 data, in the US, 60 Mt of fly ash was produced out of over 125 Mt of coal-combustion products (American Coal Ash Association, 2011 [4]. It is estimated that worldwide recycling of fly ash is only about 25% of the fly ash generated each year [5].

FA is generally grey in color, abrasive, mostly alkaline, and refractory in nature [6, 7]. The chemical composition of FA has a high percentage of silica (60– 65%), alumina (25–30%), and magnetite, Fe_2O_3 (6–15%) [6]. The American Society for Testing and Materials has classified fly ash into two classes – class F fly ash (FFA) and class C fly ash (CFA) [8]. The class C fly ash refers to those having more than 8% CaO and is usually from lignite and subbituminous coal combustion. The class F fly ash is from bituminous and anthracite coals and has less than 8% CaO [5].

There are many reasons to increase the re-utilization of fly ash [1, 6, 7]. A few of these reasons are: (a) disposal costs are minimized; (b) less area is reserved for disposal, thus enabling other uses of the land and decreasing disposal permitting requirements; (c) there may be financial returns from the sale of the by-product or at least an offset of the processing and disposal costs; and (d)

the by-products can replace some scarce or expensive natural resources. Therefore, it has become necessary to find sustainable solutions for its utilization rather than land disposal to minimize the environmental challenges associated with its disposal [6]. FA can partly replace Portland Cement (PC) in hardened concrete [9-11]. FA usage in structural concrete as a replacement of PC is around 30% of the binder. The resulting concrete has similar or enhanced performance compared to that of Portland Cement concrete which is equivalent to 28 day strength [11]. However, in order to promote wide scale usage of FA, it is critical to develop cementitous materials mainly composed of FA.

It is well known FA can also be activated by alkali to form hardened solid by geopolymerization [12-20]. The alkali activation of waste materials is a chemical process that allows the user to transform glassy structures (partially or totally amorphous and/or metastable) into very compact well-cemented composites [18]. In general, two types of cementitious materials can be produced by alkaline activation: (a) Si and Ca based, and (b) Si and Al based. The alkali activation of metakaolin or type F fly ashes (FA) is a typical example of the second situation [14]. Geopolymers are also a promising binder material to replace Ordinary Portland Cement (OPC) [12]. Most of the research to date has been conducted using class F fly ash [15, 19, 20]. A few research studies have focused on synthesizing geopolymer from Class C fly ash [16, 17]. Nevertheless, in all the studies, a high concentration of alkali solution is used to activate the mix.

The usage of large amounts of alkali activators raises several concerns, however [13]. First, the production of large amounts of alkali is an energy intensive process and can indirectly lead to increased toxic CO_2 emissions. Second, free alkali and silicate can have deleterious effects on concrete in poorly formulated systems. Therefore, it is imperative to develop fundamental

understanding whether the FA based cementitious materials can be fabricated with low or no alkali solutions.

The author proposes a "Green Cement Paradigm (GCPa)" during this study. The main components of this paradigm are: (a) use environmentally friendly precursors and aggregates, (b) minimize or eliminate the usage of alkali or other harmful chemicals as an activator, (c) usage of environmentally friendly practices for example, low w/c (w-water, c- cement) ratio etc., and (d) create a cementitious network composed of hydraulic and carbonate bonds for faster ASTM approval.

In order to validate the GCPa, Class C FA was chosen as a precursor. Recently, Gupta and Riyad [21] showed that Class C FA can have cementitious behavior if the cold pressed compacts are cured with tap water. In chapter three the mechanical behavior, microstructure analysis, and detailed phase characterization of the cementitious materials formed by using Class C FA as a reactive precursor has been reported.

Fly ash has been categorized as pozzolan [6]. Pozzolans have the capacity to react with lime in the presence of moisture and can form calcium silicate and aluminate hydrates with cementing properties [6]. Pozzolans are highly enriched with reactive silica or alumina [22] that can readily dissolve in an alkaline solution and suffice as geopolymer precursors [23]. In general, geopolymers harden with time which might take several weeks for higher strengths. Several methods have been proposed for decreasing the hardening time and also for improving the strength as well. Fly ash based geopolymers gain strength at a slower rate at ambient temperatures of around 25° C [16]. It has been suggested to cure the geopolymer at 40° – 75° C for enhancing the strength [24]. Some researchers have enhanced the geopolymerization reactions by microwave curing which led to the

requirement of less processing time [25, 26]. This might be referred to the fact that fly ash needs higher activation energy, and the added heat to the system enhances the hardening of the geopolymer as a type of thermosetting material [27]. Puertas et al. [28] reported that at ambient temperature, the reaction of fly ash was extremely slow. Several researchers have reported that the initial curing at elevated temperatures between 40° and 95° C enhances the geopolymerization and also increases the compressive strength of the geopolymer [27-30].

Prolonged grinding [31] and chemical activation [32] techniques have been used to enhance the properties of fly ash based geopolymers. Industrially produced quicklime can be used to activate both low and high calcium fly ash [33]. Temuujin et al. [34] have reported the synthesis of geopolymers at ambient temperatures by introducing the slag or calcium rich sources. It has been reported that the addition of 4 wt% of high-calcium containing slag can greatly improve the compressive strength of fly ash based geopolymers [35]. Huang and Cheng [32] have reported that the addition of hydrated lime accelerated the reaction degree of fly ash in the system during the early and later period of curing time. The rate of strength gain and the ultimate strength of lime-treated fly ash are highly dependent upon the curing temperature [32, 36]. Antiohos et al. [37] reported that the addition of 3-5% quicklime to a fly ash-cement system accelerates the hardening process and increases the strength. Some researchers have added lime into the fly ash-cement blend as hydrated form [38-40] and in slurry which provided very promising results. Shi et al. [40] investigated the effect of adding quicklime, and he also made a comparison of the effect of additional hydrated lime and quick lime in natural pozzolan-cement systems. He concluded that adding quicklime enhances the strength of the cement significantly higher than adding hydrated lime at all ages of curing.

Fly ash can be used also as a potential material for carbon di oxide capture and storage (CCS) as it contains CaO which can be carbonated in the presence of CO_2. The primary technology of carbon capture using fly ash is based on mineral carbonation due to the high content of alkali components in fly ash which are essential materials for the carbonation [40, 41]. Researchers have introduced different techniques for CO_2 capture and storage using fly ash. In wet technology, several components of fly ash such as Ca, Na, Mg and K are leached by aqueous solution and then carbonated in the presence of CO_2 [42-49]. Fly ash and some additives can be used as direct CCS materials in dry process [8, 50-52]. The dry process can be carried out in atmospheric or high pressurized conditions [53]. Soong et al. [44] and Muriithi et al. have studied the carbonation potential of coal combustion fly ash [47], and have reported that the carbonation occurs in two successive reactions. The lime presence in the fly ash is hydrated and then the spontaneous carbonation of the calcium hydroxide is occurs.

In the chapter four, the effect of high temperature curing, effect of lime content and carbonation on the cementitious materials formed by using class C fly ash have been reported. The detailed investigations of compressive strength under different conditions has been investigated and the microstructure analyses and phase characterization of the materials have also been documented.

Lignin is an amorphous natural polymeric material which is the second most abundant polymer in the world, after cellulose [54] . It is a co-product of the bio-ethanol production and paper pulping process [55], but it can be found in all plants like rice and straw. The approximate amount of lignin on the earth is about 300Gt [56]. Though it is the second most abundant polymer in the world, the industrial applications of lignin are rather limited. It has been mostly used as fuel

to produce energy [57]. However, lignin has various properties that make it suitable for different technical purposes. Lignin can be used as a stabilizer (antioxidant) for plastics and rubber [58], and also can be mixed with salts to be used as flame retardant additives for polypropylene [59-61]. The effect of lignin on the thermal behavior of various composites based on crystallizable polymers was also reported [62-66].

The phenolic base structure of lignin makes it a suitable compound to be used in polymeric materials for enhancing the mechanical properties when incorporated in a plastic [67]. Lignin also helps to improve the electrical resistance in polyolefins which makes them a potential material for use in electrical shielding applications [68]. Lignins are used as fillers in phenol formaldehyde resins, polyurethanes, polyvinylchlorides (PVC), polypropylenes, polyethylenes, polyhydroxyalkanoates and polylactides [69]. However, the complex macromolecular structure lignin has created some challenges to use it in polymer applications [70]. The thermal degradation of lignin occurs at temperatures greater than 170° C and the properties are dramatically reduced as well [71]. Therefore, it is difficult to process lignin at higher temperatures. But, it can be used for thermoset polymers which are cured below the degradation temperature of lignin [54]. The performance of lignin polymers and composites has been studied by Wool and Sun [19]. Alexy et al. [72] has also reported about the effects of blending lignin with polyethylene and polypropylene on the processing stability, light stability, long-term heat stability and mechanical properties. It has been found that the tensile strength of polymers gradually decreases with increasing amounts of lignin.

In this study, high density polyethylene (HDPE) – lignin composites have been prepared, where the content of lignin has been varied up to 35 v%. The mechanical properties of the samples have been reported in chapter five.

CHAPTER II
EXPERIMENTAL DETAILS

2.1 Sample Preparation:

Class C fly ash powder was procured from Headwaters Resources, Sioux Falls, SD. Table 1 summarizes different compositions and w/c ratio of different compositions. All the compositions

Table 1: Design compositions of class C FA based cements

Composition	Processing	Class C FA (g)	Water (g)	Sand (g)	w/c
A-1	Cold Pressed	18	3	0	0.17
B-1		20	4	20	0.20
C-1	Cast	25	6	0	0.24

were mixed in a ball mill (8000 M, SPEX SamplePrep, LLC, Metuchen, NJ) for 2 minutes. Compositions A-1 and B-1 were then cold pressed in a cylindrical steel die (~25.4 mm diameter, MTI Corp., Richmond, CA) by using a Carver Laboratory press (Model 3853, Carver Inc., Wabash, IN) at different compaction stresses of ~17 MPa, ~86 MPa and ~173 MPa, respectively. For comparison, composition C-1 (a composition similar to composition A) was cast in ~25 mm molds by vibrating the slurry on a vibrating table (PJT-100, Vibco Inc., Wyoming, RI). The

Table 2: Design composition of class C FA and $Ca(OH)_2$

Composition	Processing	Class C FA (g)	$Ca(OH)_2$ (g)	Water (g)
A-2	Cold Pressed	18	0	3
B-2		17.5	0.5	
C-2		17	1	
D-2		14.4	3.6	
E-2		10.8	7.2	

following compositions (Table 2) have been made at a compaction stress of ~86 MPa for investigating the effect of high temperature curing, additional lime content and carbonation.

For the compositions of table 2, class C FA powder and $Ca(OH)_2$ powder (molecular weight: 74.09 gm/mol, SIGMA ALDRICH) were dry ball milled (8000 M mixer Mill, SPEX SamplePrep, Metuchern, NJ) with polymethyl methacrylate (PMMA) balls for 2 minutes. After dry mixing, 3 gm of water was added, and then the mixture was mixed for 2 minutes.

For high temperature curing, the prepared samples were placed inside an aluminum foil pans and then covered completely with aluminum foil so that the moisture content inside the samples could not escape. The samples were then put inside a drying oven and cured for 24 h at a temperature of 50º C, 70º C and 90º C respectively.

A set of three samples were fabricated for each condition, and were then cured in a closed chamber for a desired number of days. Prior to and after the curing period, the mass, the height and the diameter of the samples were recorded.

High density polyethylene (HDPE) (ultra-high molecular weight, average Mw 3,000,000-6,000,000) and lignin (density 1.3g/mL at 25° C) were used for fabricating the composite samples. The HDPE-lignin composites were designed by adding 10 vol% (HDPE(90)-lignin(10)), 20 vol% (HDPE(80)-lignin(20)) and 35 vol% (HDPE(65)-lignin(35)) lignin in HDPE matrix, respectively. The compositions are presented in the table 3. For comparison, pure HDPE samples were also prepared under similar conditions.

All the compositions were dry ball milled (8000 M mixer Mill, SPEX SamplePrep, Metuchern, NJ) with polymethyl methacrylate (PMMA) balls for 2 minutes. The mixed powders were then

cold pressed in a cylindrical steel die (~25.4 mm diameter, MTI Corp., Richmond, CA) by using a Carver Laboratory press (Model 3853, Carver Inc., Wabash, IN) at a uniaxial compaction stress of ~86 MPa. All the samples were manufactured by heating at 15° C/min to 195 C, and then hot pressed at ~86 MPa for 2 minutes. The samples were allowed to cool down to 65° C and then demolded.

Table 3: Design compositions of HDPE-Lignin Composites

Composition	HDPE (g)	Lignin (g)	V_{lignin} (%)
A-3	2.06	0	0
B-3	1.77	0.26	10%
C-3	1.57	0.53	20%
D-3	1.28	0.94	35%

2.2 Carbonation Experiment Setup:

For carbonation experiment, a set of three samples were prepared for each composition (table 2) and then dried at 100º C for 24 h in a drying oven. The weight of the samples before and after the drying was measured. The dried samples were then placed inside of an autoclave chamber (Model 25 X-1, Wisconsin Aluminum Foundry Co., INC., MANITOWOL, WI).The setup is shown below in the Figure 1.The chamber was partially filled with 4 liters of water. The chamber was closed and the temperature was raised to 87º C and CO_2 gas (UN 1013 CO2 PRAXAIR INC, DANBURY, CT) was then allowed to pass inside the chamber at ~599.84 KPa for 3 h. After ~5 min the gas from the chamber purged for 2 times through the valve to ensure that no air remains

inside the chamber. After 3 h, the samples were taken out from the chamber and were dried again at 100º C for 24 h in a drying oven. The weight of the dried carbonated samples was measured. The amount of absorbed carbon di oxide was measured in gm from the dry mass difference of the dried samples before and after the carbonation.

Figure 1: Carbonation Chamber Setup

2.3 Sample Characterization:

2.3.1 Green Density & Pore Size Distribution Measurement of Class C Fa Samples:

For measuring the green density of class C FA samples, a separate set of five samples were prepared under different compaction stresses, and then dried at 100º C for 24 h in a drying oven. The weight of the samples before and after the drying was measured. The green density (ρ_g) was then calculated from the dry mass and the volume. The theoretical density (ρ_T) of the fly ash

powders was measured by He pycnometry (Ultrapycn 1200e, Quantachrome Instruments, Boynton Beach, FL). The total porosity (P) and relative density (ρ_r) was calculated from Eq. 1.

$$P = (1- \rho_r) = (1- (\rho_g/ \rho_T)) \times 100 \text{ ----------(1)}$$

The pore size distribution was measured by Hg porosimetry (PoreMaster 60, Quantachrome Instruments, Boynton Beach, FL).

2.3.2 Mechanical Characterization:

The compressive strength of the samples was measured by a mechanical testing system Shimadzu AG- IS UTM (Shimadzu AG-IS UTM, Shimadzu Scientific Instruments Inc., Columbia, MD) at a deflection rate of 1 mm/min. The compressive strength was reported for an average of 3 samples for all design compositions of class C FA samples. The aspect ratio of the compositions A and B were ~0.7 and ~1.0 (Table 1), and for all the compositions of Table 2 was ~0.7 approximately.

The HDPE-Lignin composite samples were machined into ~3 mm cubes for compressive testing. For each composition, a set of 5 samples were tested at a deflection rate of 0.5 mm/min. It was not possible to measure the actual strain of each sample accurately, hence stress versus displacements are reported. For qualitative comparison, an average of 5 yield strength measurements for each composition is reported. The linear region had a regression fitting of $R2 > 0.95$ in the stress versus displacement plots.

The 3 point flexural bending test was done for the HDPE-Lignin composite samples. The samples were cut to dimensions ~22 mm long, ~2 mm thick and ~4 mm wide. For each

composition, a set of 5 samples, were tested at a deflection rate of 5mm/min in Shimadzu AG- IS UTM (Shimadzu AG-IS UTM, Shimadzu Scientific Instruments Inc., Columbia, MD).

2.3.3 Microstructure Investigation:

For microstructure analysis, the samples were coated with Au/Pd by using a Balzers SCD 030 sputter coater (BAL-TEC RMC, Tucson AZ, USA), and then mounted on aluminum mounts. Secondary electron (SE) and Backscattered Electrons (BSE) images were obtained using a JEOL JSM-6490LV Scanning Electron Microscope (JEOL USA, Inc., Peabody, Massachusetts).

2.3.4 Phase Analysis:

Both XRD and TGA/DSC analysis was done for the characterization of the class C FA samples (table 1 and 2). XRD patterns were collected from 20-60º (2θ) by using a Rigaku Ultima IV X-Ray Diffractometer (Rigaku Americas, The Woodlands, TX). Crystalline phase were identified by computer search-match procedures, which employ the ICDD Powder Diffraction file, using MDI Jade 9.0 Software.

For TGA/DSC (SDT Q600, TA Instruments, New Castle, DE) analysis, the fractured pieces of the samples were collected, and crushed into fine powders. A small amount of powdered sample (~75 mg) was placed inside the TGA/DSC instrument. Initially, the furnace was heated at 10º C/min to 1000º C from room temperature (RT), and then it was cooled to RT

CHAPTER III
ON THE USAGE OF CLASS C FLY ASH AS A SOLE SOURCE OF CEMENTITIOUS PHASE

3.1 Effect of Compaction Stress on the Compressive Strength

Figure 2 shows the variation of compressive strength of different compositions after curing for different number of days. During this study, all the samples were fabricated at a compaction stress of ~86 MPa. For composition A-1 (Table 1), the compressive strength increased sharply to ~20 MPa after 1 day, thereafter gradually increased to ~29.5 MPa after 28 days. The compressive strength of the samples remained almost same after 56 days (Figure 2 a). This results show that Class C is almost completely cured by 28 days. The composition B-1 (Table 1) also showed similar trend but the final compressive strength was ~19 MPa after curing for 28 days (Figure 2 b).

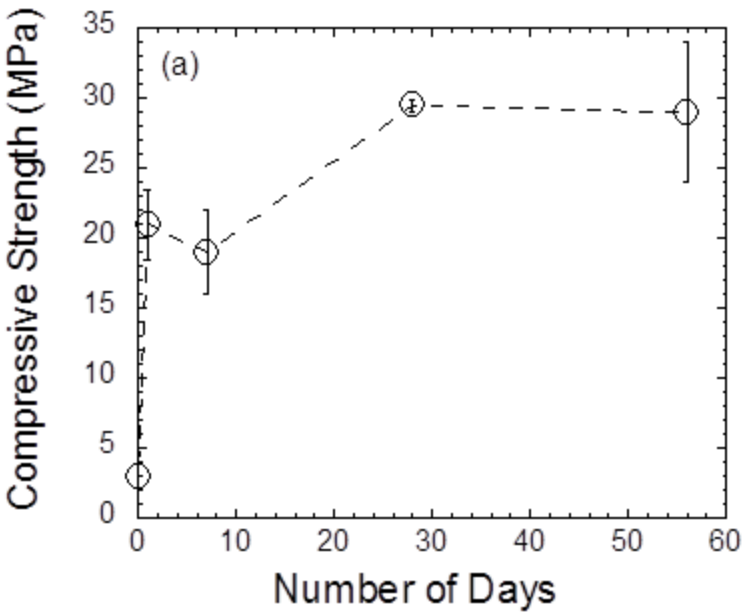

"Figure # cont."

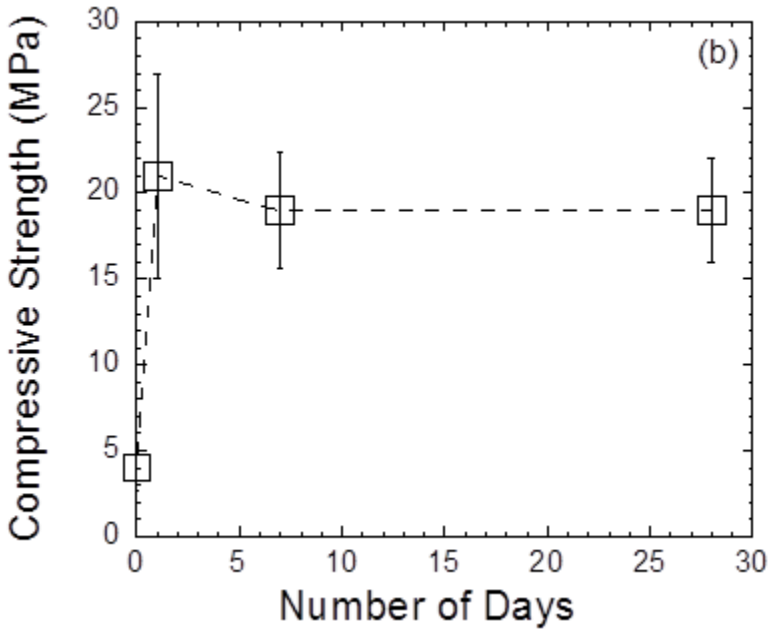

Figure 2: Variation of compressive strength of, (a) Class C Fly Ash (Composition A-1, Table 1) and (b) Class C Fly Ash – sand composites (Composition B-1, Table 1) as a function of number of days. All the samples were prepared at a compaction stress of ~86 MPa

Composition A-1 (Table 1) was further investigated at different compaction stresses. Figure 3 shows the variation of relative density as a function of compaction stress. For comparison, the cast samples (Composition C-1, Table 1) had a relative density of ~60%, and the relative density gradually increased to ~70% and ~72% as the compaction stress was increased to ~17 MPa and ~86 MPa, respectively. Thereafter, the relative density retained similar value as the compaction stress was further increased to ~173 MPa.

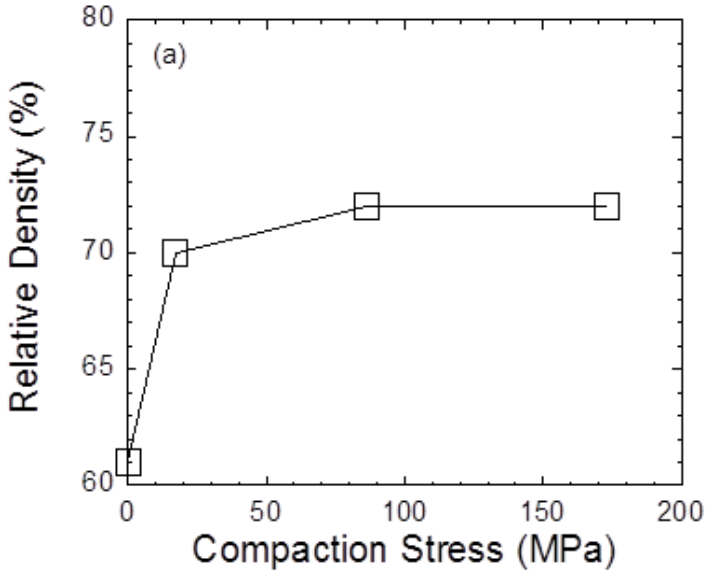

Figure 3: Variation of relative density as a function of compaction stress of Class C FA (Composition A-1, Table 1).

Figure 4 shows the effect of variation of the compaction stress on the compressive strength of composition A-1 (Table 1) after curing for 7 and 28 days, respectively. For comparison, results of composition C-1 (Table 1) are also included in the plot. After 7 days of curing, the compressive strength increased from ~5 MPa to ~21 MPa as the compaction stress was increased from 0 MPa to ~17 MPa, thereafter, the compressive strength of the samples retained similar values as the compaction stress was further increased to ~86 MPa and ~173 MPa, respectively. Interestingly, after curing for 28 days, the compressive strength gradually increased to ~21 MPa and ~32 MPa as the compaction stress was increased to ~17 MPa and ~86 MPa, respectively. Further increase in the compaction stress did not have any enhanced effect on the compressive strength as the relative density did not change significantly with compaction pressure.

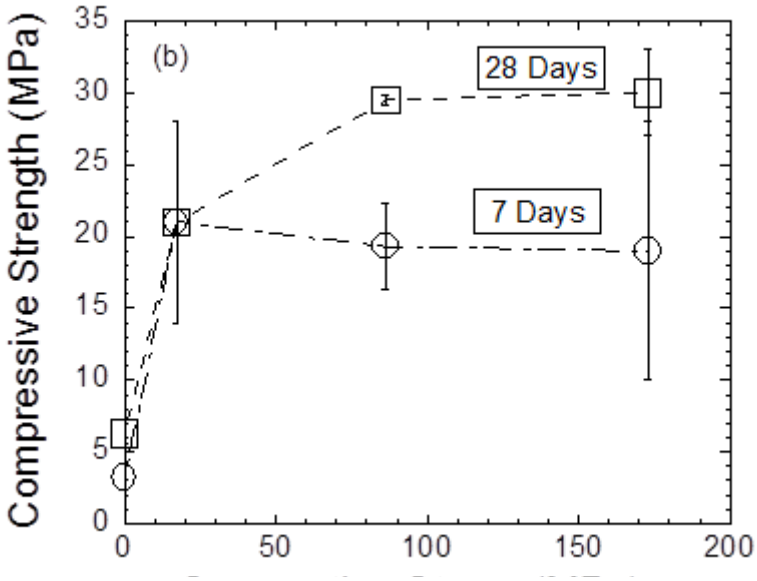

Figure 4: Variation of compressive strength as a function of compaction stress of Class C FA (Composition A-1 ,Table 1).

The effect of porosity on the compressive strength of ceramic and cement based materials are well studied [73-79]. There are different mathematical models to model the evolution of compressive strength with porosity. Ryshkewitch [78] proposed an exponential mathematical relation (2) from the study of the compressive strength of Al_2O_3 and ZrO_2.

$$\sigma = \sigma_0 e^{-kp} \text{----------(2)}$$

where σ is the strength, σ_0 is the strength at zero porosity, and *k* is the empirical constant.

Hasselman [75] proposed a linear relationship between strength and porosity for different refractory materials (Eq. (3)):

$$\sigma = \sigma_0 - cP \text{----------(3)}$$

where *c* is the empirical constant.

Figure 5 plots the increase in compressive strength as a function of porosity of composition A-1 (Table 1) after curing for 28 days. Figure 5 also shows the mathematical fitting of Ryshkewitch and Hesselman model. The exponential functions show a better fit. The evolution of compressive strength (σ_c) can be empirically modeled by using an exponential function (Eq.2).

$$\sigma_c = \alpha e^{-\beta P} \text{ ----------(4)}$$

where, α and β are empirical constants.

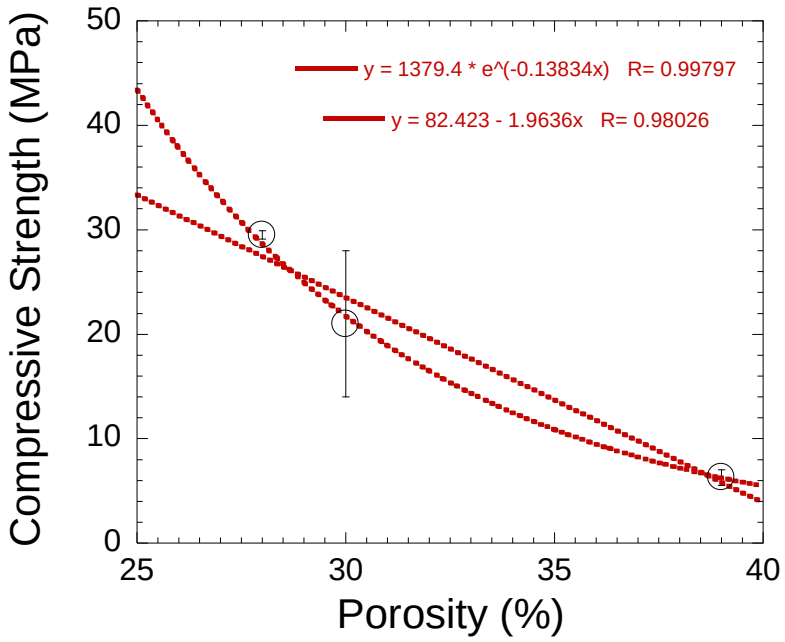

Figure 5: Variation of compressive strength of cured FA samples (Compostion A-1, Table 1) as a function of porosity (P).

The author would like to acknowledge that more studies are needed to completely understand the evolution of compressive strength with porosity in this system. However, as shown in Figure 2, it is not possible to attain higher relative density by using compaction stresses, thus for future studies particle size engineering approach is recommended [80]. Nevertheless, this study further confirms that the compressive strength is highly dependent on relative density. Figure 6 shows a typical pore size distribution of composition A-1 (Table 1) cold pressed at ~86 MPa and cured for 28 days.

The pore size distribution is continuous and most of the pores are mainly concentrated between ~100 nm and ~1 µm.

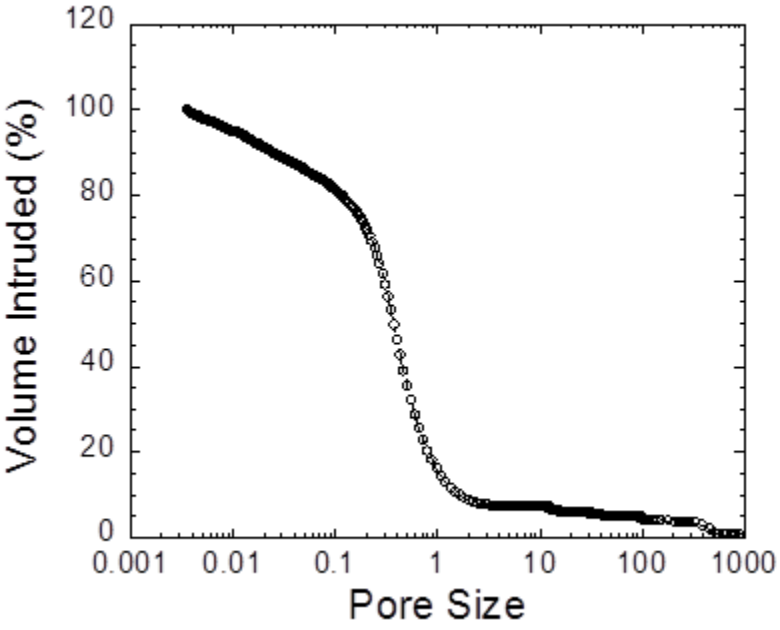

Figure 6: Pore size distribution of Class C FA cold pressed at ~86 MPa and cured for 28 days (Composition A-1,Table 1) by Hg porosimetry.

3.2 Microstructure and Phase Analysis

Figure 7(a) shows the SEM micrograph of as received class C fly ash sample. The sample is composed of spherical particles of different dimensions. Figure 7b shows the fractured surface of cold pressed class C fly ash after curing for 28 days. Figures 7(c) and 7(d) show the higher magnification of the same region in secondary electron (SE) mode and backscattered electron (BSE) mode, respectively. By analyzing the Figures 7 b-d, we can construe that micron sized needle shaped particles are cementing the FA particles together. Figure 7 (e) shows the morphology of needle shaped particles at higher magnification. Due to finer dimensions of these particles, it is difficult to accurately determine the composition of these phases by EDS analysis.

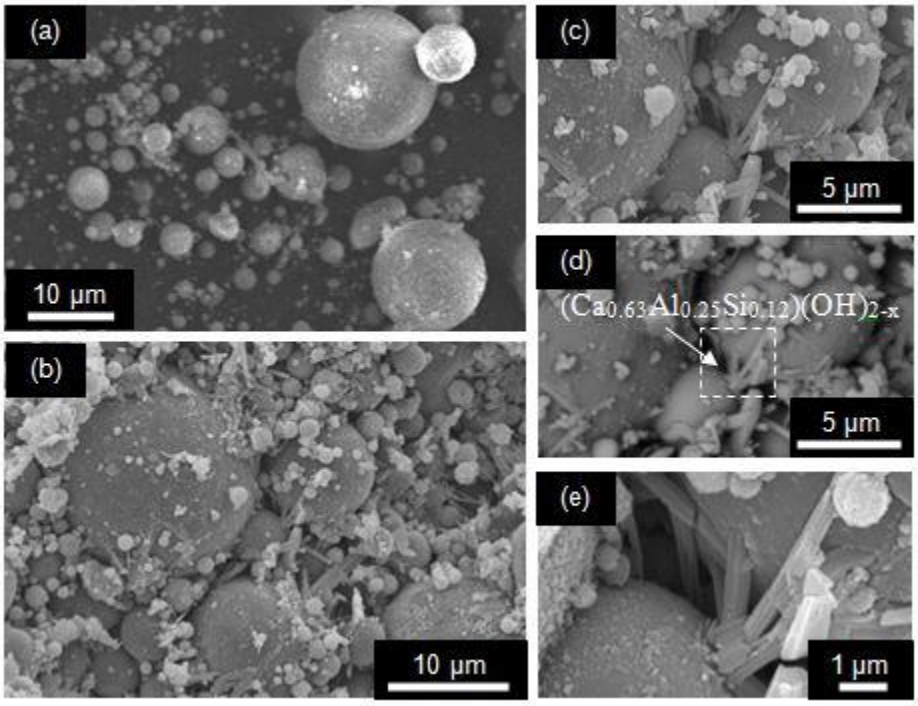

Figure 7: SEM micrographs of, (a) as received Class C Fly Ash, and Au-Pd coated fractured surface of Class C FA cold pressed at ~86 MPa and cured for 28 days (Composition A-1,Table 1), (b) in Secondary Electron (SE) mode; higher magnification of the same region in (c) SE, (d) Backscattered Electron (BSE) mode, and (e) SEM micrograph of the hydrated region A in (d).

For qualitative understanding, the chemical composition of these particles by EDS analysis is $(Ca_{0.63}Al_{0.25}Si_{0.12})(OH)_2$. Thus, qualitatively we can conclude that the needle shaped particles are mainly composed of Ca-rich hydrates although the exact stoichiometry of these particles is uncertain at this juncture (Fig. 6d).

Figure 8 shows the thermo gravimetric analysis (TGA) of as received Class C Fly Ash and cured fly ash after 28 days. During heating of the cured class C Fly ash sample, ~3.1 wt% weight loss is observed until 200^{o}C. The weight loss can be attributed due to the loss of moisture, capillary water, and decomposition of C-S-H (Calcium Silicate Hydrate) phases from the sample [80]. A

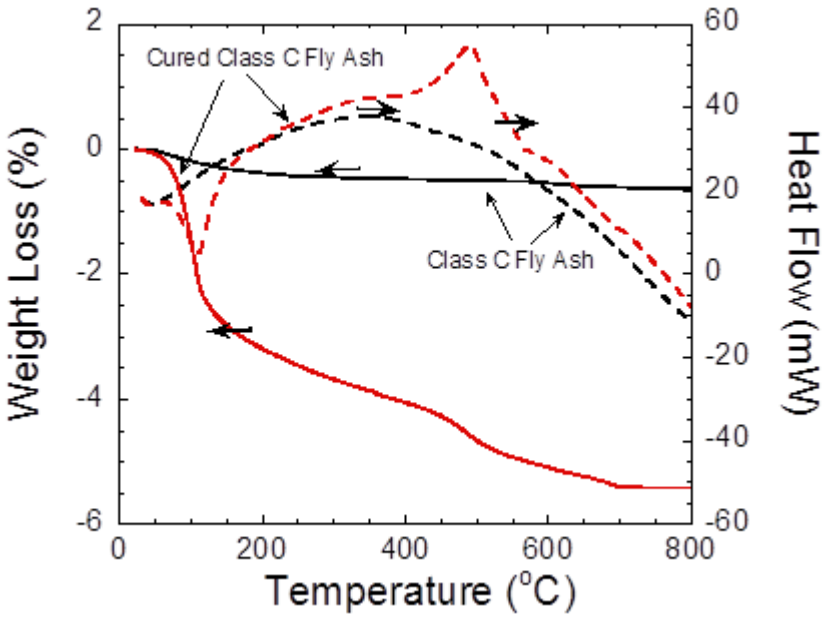

Figure 8: DSC/TGA of as received Class C FA and Class C FA cold pressed at ~86 MPa and cured for 28 days (Composition A , Table 1). The red color represents composition A, and the black color represents as received Class C FA. The solid line represents TGA data, and the dotted line represents DSC data.

peak in DSC is also observed at 480°C. It is well established that $Ca(OH)_2$ also decomposes at similar conditions [80]. Similar peak was not observed in pure FA samples. Thus, the peak can be attributed to the decomposition of Ca-rich hydrates. This result further supports the conclusion that needle shaped particles are composed of Ca-rich hydrates.

X-ray powder diffraction patterns of FA and FA samples cured for 28 days are shown in Figure 9. The XRD patterns of both compositions are almost identical. The major crystalline phases are Mullite ($3Al_2O_3.2SiO_2$), Quartz (SiO_2), and anhydrite ($CaSO_4$). From TGA studies, we can conclude that the concentration of needle shaped hydrated Ca-rich phases are low (Figure 8). Needle shaped particles hydrated Ca-rich phases are also nanocrystallaine (Figure 7e). Due to these reasons, XRD was not able to detect these phases.

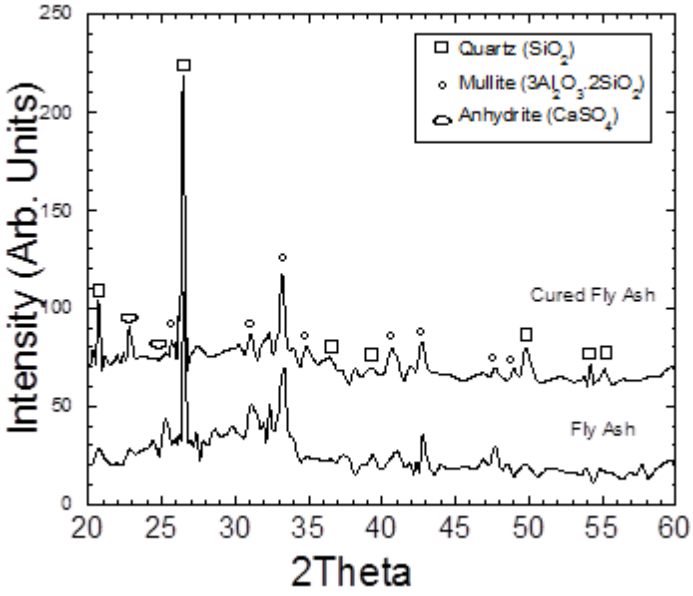

Figure 9: XRD of as received Class C FA and Class C FA cold pressed at ~86 MPa and cured for 28 days (Composition A-1,Table 1).

3.3 Potential Mechanism

The beneficial effect of pressure and low w/c ratio on conventional PC Concrete is well known [73-75, 77-79, 81]. The fundamental reason is due to the decrease in porosity at higher compaction pressures. Zivica et al. [79, 81] surmised that low-porosity cement composites have a great potential in modification of composition and subsequently structure of the cement based materials. Freidin et al. [27] also reported the beneficial effect of the compaction pressure on the mechanical performance of Alkali Activated FA compositions.

By analyzing all the supporting data, we can construe that the synergistic effect of compaction and hydration is responsible for the enhanced strength in these solids. More studies are needed to understand the complex hydration mechanisms of Class C FA.

3.4 Conclusions

The compressive strength is dependent on the relative density of the samples. The relative density can be tailored by the compaction stress. The compressive strength changed exponentially with porosity. The number of curing days also played a significant role in the increase of the compressive strength. The experimental results indicate that the curing for 28 days is the optimum time for strength development.

From the SEM micrograph, we can observe the micron-sized needle-shaped Ca-rich hydrates form the main cementitous network in these solids. The TGA/DSC results also support the formation of Ca-rich hydrated phase. Overall the results showed that Class C Fly Ash can be a sole source of cement precursor.

CHAPTER IV
NOVEL ENGINEERED CEMENTITIOUS MATERIALS BY CLASS C FLY ASH

4.1 Effect of Temperature on Compressive Strength

Figure 10 shows the effect of temperature on the mechanical strength of composition A-2 (Table-2). The compressive strength of the sample was found to be ~30 MPa after 28 days of curing at room temperature. On the other hand, all other samples have been cured at higher temperature for 3 h. The samples have been cured for 3 h at 50º C and 70º C respectively had a similar compressive strength of ~30 MPa. A higher compressive strength of ~45 MPa has been observed for the samples that have been cured at 90º C. So we can conclude that, at high

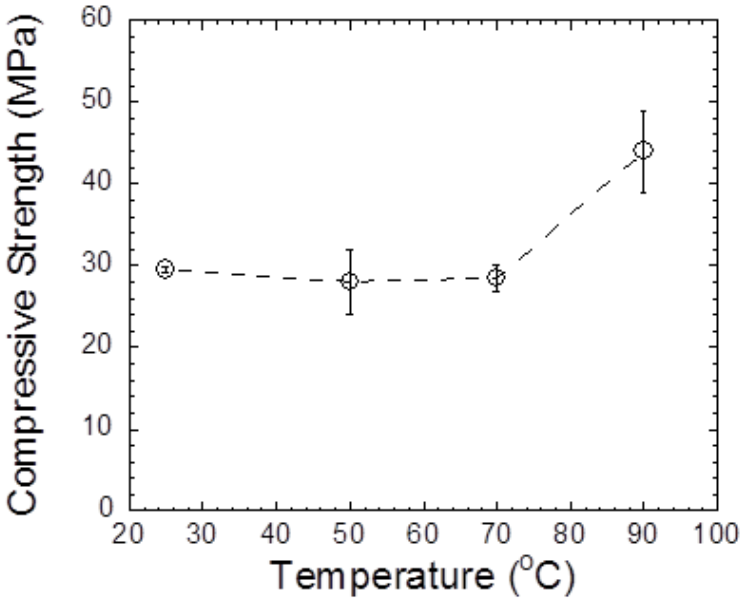

Figure 10: Effect of temperature on the mechanical strength. The samples studied at RT was cured for 28 days, whereas all the other samples were cured at the designated temperature for 3h

temperature curing we can achieve a good compressive strength of the samples within a short period of time.

4.2 Effect of Additional $Ca(OH)_2$ on Compressive Strength

Figure 11 shows the effect of adding calcium compounds on the compressive strength of the samples prepared from Class C Fly Ash. $Ca(OH)_2$ was substituted at 2.78, 5.5, 20 and 40 wt% for fly ash in the samples. The samples were prepared at a compaction stress of ~86 MPa

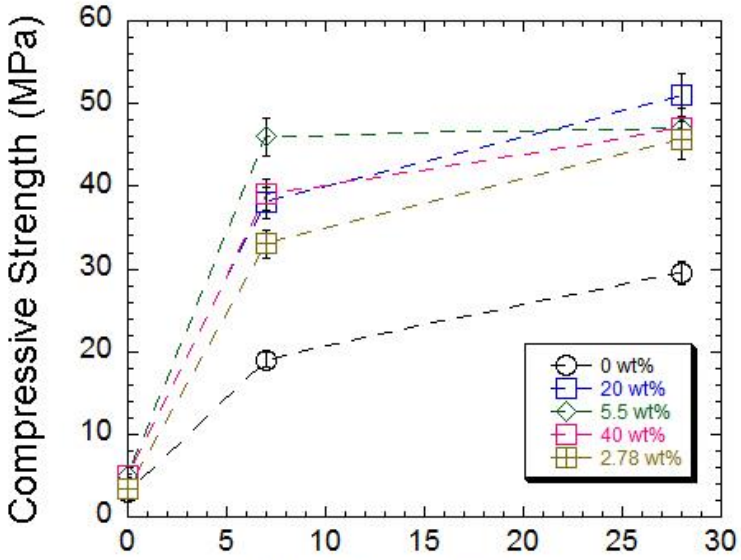

Figure 11: Effect of additional $Ca(OH)_2$ on the compressive strength of samples (Table 2)

and cured for 0, 7 and 28 days respectively. From Figure 11, we can see that the addition of $Ca(OH)_2$ has enhanced the compressive strength of the samples for all design compositions (Table 2). Though the initial strength of the green bodies for all compositions was at ~5 MPa, after 7 and 28 days curing, we can see a significant enhancement of the compressive strength for all the samples with additional $Ca(OH)_2$. After 28 days curing, the compressive strength was increased to ~45 MPa for all the samples containing $Ca(OH)_2$.

4.3 Effect of Carbonation on the Compressive Strength

Figure 12 shows the comparison of the compressive strength of the class C FA samples (Table 2) treated under different conditions. The addition of $Ca(OH)_2$ and high temperature curing followed by the carbonation have increased the compressive strength of the samples significantly. The carbonation contributed to the development of compressive strength. For example, the samples made from class C FA only had a compressive strength of ~40 MPa after carbonation, whereas after 28 days of curing the compressive strength for the same composition was ~30 MPa. For the rest of the compositions, we can also see a significant strength development after carbonation. The heat treatment followed by carbonation significantly contributed to the enhancement in compressive strength. For example, the composition E-2 (table 2) had a maximum

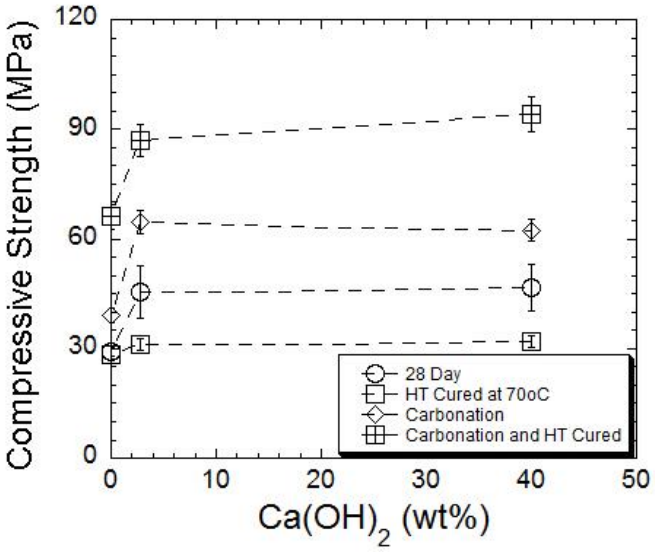

Figure 12: Comparison of the compressive strength of the samples treated under different conditions

compressive strength of ~92 MPa after both high temperature curing and carbonation. Therefore, we can conclude that both carbonation and high temperature curing enhances the compressive strength of the materials.

4.2 Microstructure and Phase Analysis

The thermo gravimetric analysis (TGA), which was carried out to evaluate the thermal behavior for different samples under different curing conditions, is presented in figure 13. During heating of as received fly ash, we see a minimum weight loss of ~0.5% which was due to release of moisture. For the rest of the samples, we have observed a weight loss from ~2 to ~4 wt% until 200º C (Stage A). The weight loss occurred probably due to the loss of moisture, capillary water,

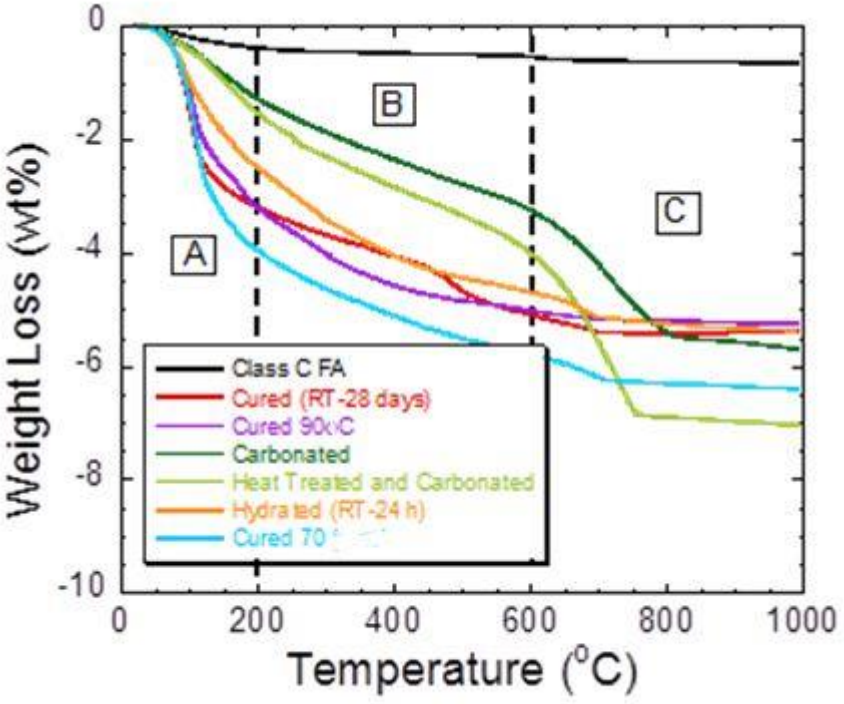

Figure 13: TGA analysis of samples cured at different conditions

and decomposition of C-S-H (Calcium Silicate Hydrate) phases from the samples. The decrease in mass is also observed around 400°C which is due to the dehydration reaction of $Ca(OH)_2$ (Stage B). A significant amount of weight loss occurred for the carbonated fly ash and heat treated carbonated fly ash samples in the temperature range of 600 - 800º C (Stage C). These weight loss phenomena can be attributed to the decomposition of $CaCO_3$ which has formed due to the

carbonation in the samples. It has been reported in several articles that decomposition of calcium carbonate occurs in between 650 to 950º C depending upon the heating rate [82-84].

X-ray powder diffraction patterns of several samples cured for 28 days are shown in Figure 14. The XRD patterns for the non-carbonated samples are quite different from all other

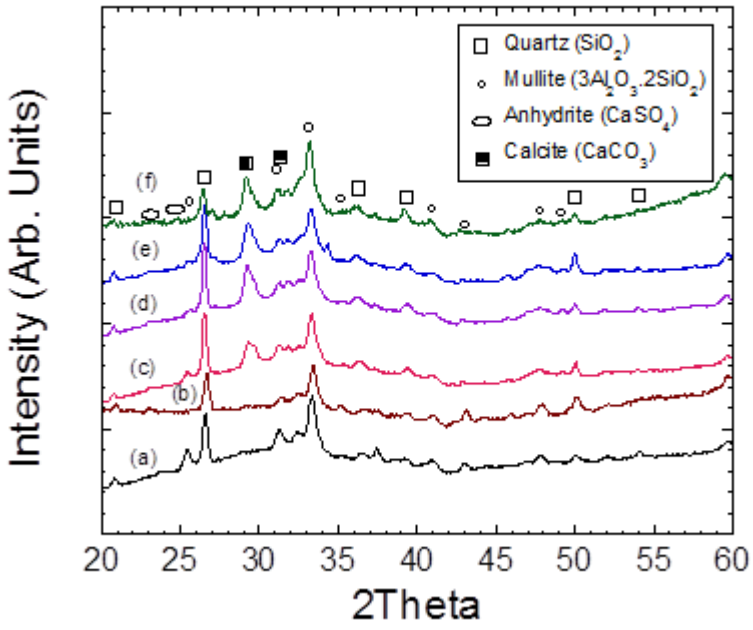

Figure 14: XRD profiles of, (a) as-received class C Fly Ash, and after, (b) heat treated at 90ºC, (c) carbonation under standard conditions, (d) heat treated at 90ºC and carbonated, (e) carbonation after addition of 2.78 wt% $Ca(OH)_2$, and (f) heat treatment at 90ºC and carbonation after the addition of 2.78 wt% $Ca(OH)_2$

carbonated samples. For all the carbonated samples under different conditions (c, d, e, f) , we can observe a peak at 30 degree which is not found for the non-carbonated samples. The major crystalline phase at that region is Calcite ($CaCO_3$) which proves that the $Ca(OH)_2$ present in the fly ash has reacted with the CO_2 during the carbonation experiment and formed carbonate. However, the major crystalline phases are Mullite ($3Al_2O_3.2SiO_2$), Quartz (SiO_2), and anhydrite ($CaSO_4$) for all the samples.

Figure 15(a) and 14(b) show the SEM micrograph of the carbonated class C fly ash sample at low and high magnification respectively. Calcite ($CaCO_3$) was observed in the XRD analysis (Figure 14) of all the carbonated samples. Figure 15 (b) clearly shows the deposition of calcite

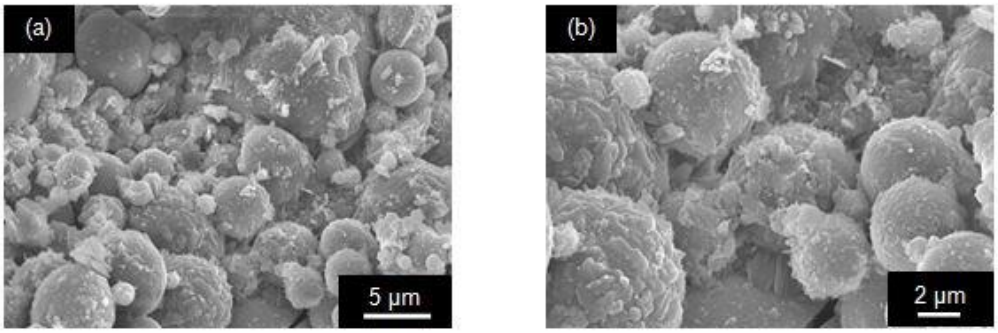

Figure 15: SEM micrographs of carbonated Class C Fly Ash at, (a) low, and (b) high magnification

particles around the bigger spherical particles. Therefore, we can construe that calcium content of class C fly ash has been reacted with the CO_2 during the carbonation process.

Figure 16(a) and 16(b) represent both the low and high magnification of SEM micrograph of the sample which has been cured at 70°C for 24 h followed by 3 h of carbonation. From the micrographs we can observe that a significant amount of crystalline structures are deposited around the spherical particles along with the calcite.

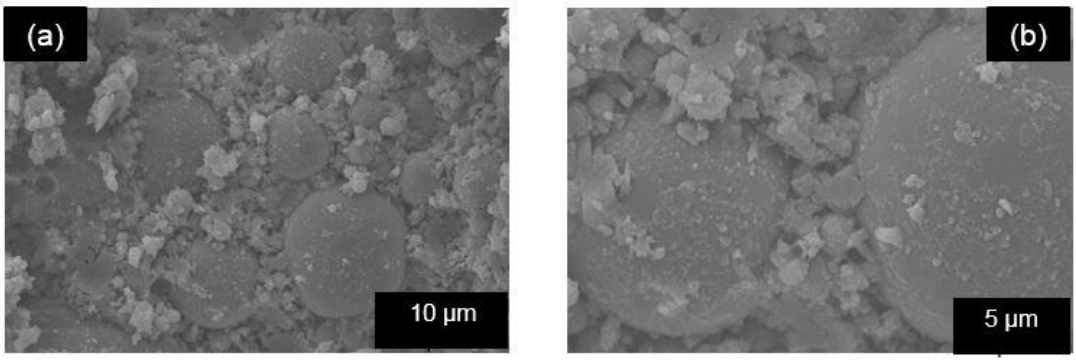

Figure 16: SEM micrographs of high temperature cured carbonated Class C Fly Ash at, (a) low, and (b) high magnification

4.3 Potential Mechanism

It has been reported that thermal treatment is an important factor for the activation of fly ash as it helps to overcome the activation barrier [85]. One of the traditional synthetic methods for making fly ash-based geopolymers also involves the mild-temperature curing for a certain period of time [86]. Rovaník et al. [87] reported that the elevated temperature curing helps to enhance the compressive strength of metakaolin-based geopolymer. Bakharev et al. [27] has also reported that geopolymeric materials prepared from Class F fly ash had an enhanced mechanical strength due to high temperature curing. For the Class C fly ash we have observed that samples cured between 50-90º C for 24 h had enhanced compressive strength. This phenomena can be attributed to the possible reason that heat might have facilitated the hydration process which can be considered as a similar to the hydration process of ordinary cement [86].

The addition of hydrated lime in the fly ash – $Ca(OH)_2$ -H_2O system helps to accelerate the reaction degree of fly ash both in the early and later ages of the curing period [32]. Shi et al. [40] has used quicklime to activate the action of natural pozzolans. He has reported that the addition of quicklime enhanced the strength of cement than hydrated lime at all ages of hydration. Anitohos et al. [33] reported that addition of quicklime in Class C Fly ash enhances the strength during the curing period. The additional lime has reacted with reactive dissolved silica from fly ash and formed additional C-S-H [33]. Due to the presence of $Ca(OH)_2$, a significant amount of soluble silica is released from the reacted fly ash particles into the matrix [88, 89]. The hydration of additional lime contributes to the formation of flocs inside the matrix and as a result it helps to enhance the strength of the system [33]. Pandian et al. [90] reported that the formation of flocs inside the matrix reduce the void spaces which leads to the minimization of the interconnectivity of pores, and therefore the microstructure gets more denser.

From figure 11, we have observed the similar trend in the compressive strength of different compositions (table 2). After 7 days of curing, we have observed a higher strength in the samples that contain 5.5 wt% of $Ca(OH)_2$. On the other hand, the samples contained 20 wt% of $Ca(OH)_2$ had the maximum strength of ~50 MPa after 28 days of curing.

Haq et al. [91] reported that carbonated fly ash Geopolymer had improved mechanical properties due to uniformity, presence of strong silica network, and higher geopolymerization. In our studies, we also have observed that carbonated fly ash samples have higher compressive strength (Figure 12). Several researchers have reported that calcite and aragonite phase usually forms due to the accelerated carbonation of coal fly ash [43, 92, 93]. In the carbonation study, calcite was identified as the only polymorph of $CaCO_3$ which formed during the carbonation process. The XRD analysis (Figure 14) and SEM micrograph (Figure 15) justifies the formation of calcite.

4.4 Conclusions

The addition of $Ca(OH)_2$, high temperature curing and carbonation had significantly enhanced the compressive strength of the samples (table 2). The curing period of the class C FA sample can be drastically reduced by high temperature curing and carbonation with an improved mechanical strength. Both high temperature curing and carbonation of the samples are suggested for the maximum improvement of the mechanical properties for all designed compositions.

CHAPTER V
HDPE AND LIGNIN COMPOSITES

5.1 Mechanical Properties of the HDPE-Lignin Composites:

Figure 17 shows the change in yield strength and flexural strength of the HDPE-lignin composites (table 3) with respect to the change of vol% of lignin in the samples. For 100 vol% HDPE sample, the yield strength was ~9 MPa, and the flexural strength was ~17 MPa. For an

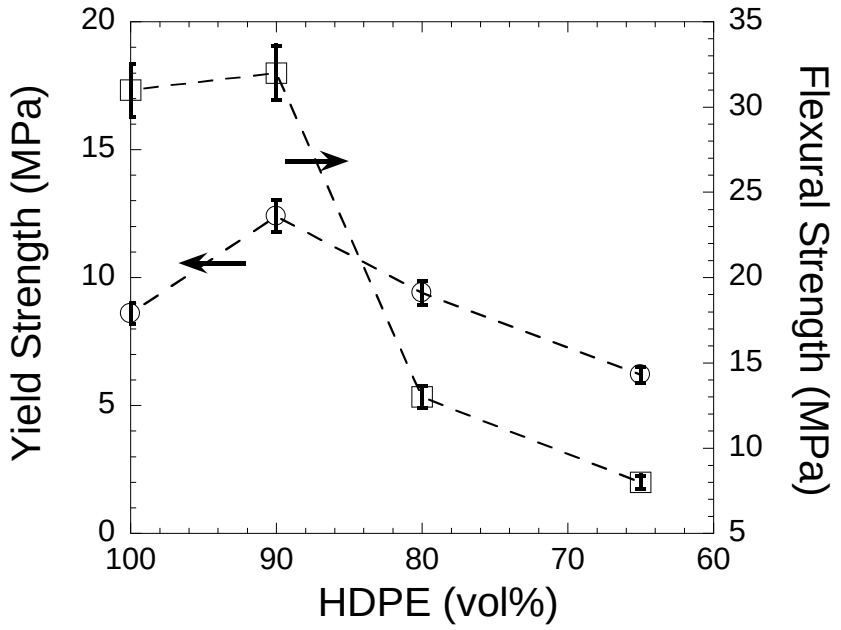

Figure 17: Variation of Yield Strength and Flexural Strength for different compositions of HDPE-Lignin composites

addition of 10 vol% lignin, the yield strength was enhanced up to ~13 MPa. The sample containing 20 vol% lignin had similar yield strength compared to the pure HDPE samples, but the flexural strength was deigraded. For further addition of lignin, we can see the degradation in both yield and

flexural strength for all the designed compositions. Therefore, we can conclude that if the lignin content is more than 20% the mechanical properties are decreased.

5.2 Potential Mechanism

For polypropylene and polyethylene, the mechanical properties decrease with increasing lignin content [72]. From figure 16, we have observed degradation in the mechanical properties of the composite samples containing more than 10 vol% lignin. This might have occurred due to the poor interaction between the lignin particles and the matrix. It has been reported that thermal degradation of lignin takes place at a temperature greater than 170° C, and the properties of lignin are dramatically reduced [71]. For the samples containing higher vol% of lignin, a significant amount of lignin might have degraded at the manufacturing temperature of 195° C which resulted in poor interaction between the lignin particles and the matrix. To establish the fact, a detailed investigation of the blend morphology of lignin and HDPE particles is recommended.

5.3 Conclusions

The experimental investigation of the HDPE-lignin composites shows that lignin can be used with HDPE to manufacture composites. Lignin helped to reinforce the polymer matrix when it was used up to 10 vol%, and for greater than 20 vol% amount of the mechanical properties of the composites have been degraded.

APPENDIX

Gupta, S. and Riyad, M. F. (2014), Oxidation-induced Sintering: An Innovative Method for Manufacturing Porous Ceramics. International Journal of Applied Ceramic Technology, 11 [5] 817-823, 2014, DOI: 10.1111/ijac.122

Int. J. Appl. Ceram. Technol., 11 [5] 817–823 (2014)
DOI:10.1111/ijac.12282

Oxidation-Induced Sintering: An Innovative Method for Manufacturing Porous Ceramics

Surojit Gupta* and Mohammad F. Riyad

Department of Mechanical Engineering, University of North Dakota, Grand Forks, North Dakota 58201

We report for the first time a novel method of manufacturing macroporous ceramics by oxidation-induced sintering (OIS) of porous compacts composed of Ti powders and fugitive poreformers. Using this novel manufacturing method, novel porous TiO_2 ceramics can be fabricated over a wide range of porosity at a relatively faster heating rate (4°C/min) and shorter sintering periods (≤4 h) at 1450°C. The porous ceramics were subsequently characterized by SEM, XRD, and compressive strength measurements. The detailed microstructure study showed that the solid network in these solids is interconnected.

Introduction

Porous materials with closed or open pores have applications in a wide range of fields, for example, ceramic filters, supports for catalysts, bone scaffolds, porous piezoelectric ceramics, electrodes in fuel cells, porous burners, lightweight load-bearing structures, etc.[1–12] The four most common methods for fabricating porous ceramic materials are as follows: (i) replication of a sacrificial foam template, (ii) direct foaming of liquid slurry, (iii) burnout of fugitive pore former from the cast samples, and (iv) partial sintering.[1,2,7] Each of these methods has its own merits and drawbacks.[1,2] Some of the fundamental issues of methods (i)–(iii) are controlling drying shrinkage, pore morphology and size, among others.

The method (iv), partial sintering method, is currently used for manufacturing porous solids with a limited range of porosities. For example, She *et al.*[9–11] had used oxidation to fabricate porous SiC ceramics. Briefly, during the oxidation-bonded SiC ceramic (OBSC) manufacturing process, SiC powders with or without additives were dry-pressed into rectangular compacts and then heat-treated in air at temperatures in the range of 1100–1500°C using a one-step heating cycle with a heating and cooling rate of 5°C/min. Due to the occurrence of surface oxidation during the heat treatment, SiC particles were bonded to each other by the oxidation-derived SiO_2 glass. For example, when ~0.6 μm SiC powders were used, a high strength of ~185 MPa was achieved at a porosity of ~31%. In future, it would be interesting to fabricate ultra-porous scaffolds (>60% porosity) by OBSC method. Thus, novel innovative methods of manufacturing porous solids are needed that can enhance the efficiency of manufacturing.

In the literature, investigators have also oxidized Ti metal to produce self-organized TiO_2 layers.[5] The scanning electron microscopy (SEM) images revealed that the TiO_2 particle layers after spontaneous delamination have porous structure. The thicknesses of the TiO_2 layers increase with increasing calcination temperature and time. Furthermore, the sizes of the TiO_2 particles depend on the calcination temperature and time.

Recently, Gupta [12] invented a novel manufacturing process, "*oxidation-induced sintering* (OIS)," for manufacturing porous ceramics by controlled bulk oxidation of porous compacts composed of Ti powders and fugitive pore formers. In this paper, we report for the first time the manufacturing process, microstructures, and the mechanical behavior of these novel ceramics. As far as we are aware, no one has reported the direct conversion of metallic precursors into porous oxide ceramics.

Experimental Details

Table I shows details about different raw materials used during this work. Table II shows different compositions used this work. Green body (porous performs) was prepared for all the compositions by mixing the powders in a ball mill (8000 *M* mixer Mill; SPEX SamplePrep, Metuchen, NJ) for 5 min. Thereafter, these powders were cold pressed in a Carver Laboratory press (Model 3853; Carver, Wabash, IN) at a compressive stress of ~86 MPa. All the samples were heated in a tube furnace at a heating rate of 4°C/min in air.

The weight and dimensions of the samples were measured before and after the heat treatment (oxidation). In the text, the longitudinal direction is defined as the direction parallel to the cold pressing direction in the die, and the transverse direction is defined as the direc-

*surojit.gupta@engr.und.edu

Table I. Specifications of Raw Materials Used During This Work

Product	Powder name	Company	Specifications	ρ (g/cm^3)
429015	Polyethylene (PE) (Pore former I)	Sigma-Aldrich, St. Louis, MO	Ultrahigh molecular weight and average M_w 3,000,000–6,000,000	0.94
332461	Graphite (Pore former II)		Flakes (+150 mesh)	2.25
43102	Titanium	Alfa Aesar, Ward Hill, MA	Powder (−200 mesh)	4.51

Table II. Composition of Different Precursors Used During This Work

Composition	Ti (g)	PE (g)	Graphite (g)	V_{fp} (%)
C	3.5	0.5	1.5	61
D	3.5	0.5	7	82
E	1.75	0.25	7	90

tion perpendicular to the cold pressing direction in the die. The dimensions (height and diameter) of the samples were measured by an electronic vernier caliper. The dimensions were then used to calculate volume of the samples before and after the heat treatment. The longitudinal and transverse shrinkages were also calculated from the measured dimensions. The green bulk density (ρ_{GBD}) and reacted bulk density (ρ_{RBD}) were calculated from the measured weight and calculated volume of the

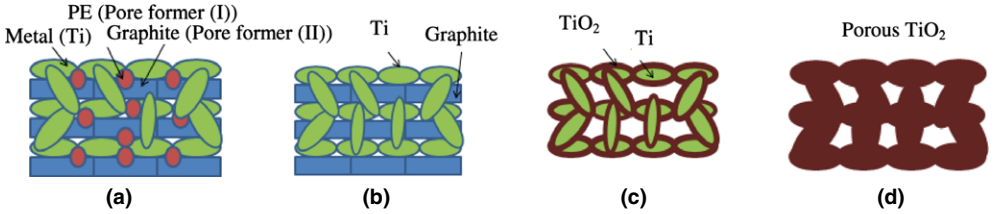

Fig. 1. Schematics of manufacturing of porous oxide ceramics by the OIS method: (a) packing of mixed powders of metal (Ti), PE ((pore former (I)), and graphite (pore former (II)) into compacts, (b) oxidation and removal of polyethylene (pore former (I)) during heating, (c) oxidation and removal of graphite (pore former (II)) during further heating and concomitant partial oxidation of Ti, and (d) formation of porous TiO_2 ceramics at higher temperatures due to the complete oxidation of metal powders.

Table III. Summary of Physical Properties of Different Porous Materials

Composition (Table II)	Temperature and time	Calculated porosity (P)	Compressive strength (MPa) (Transverse)	Compressive strength (MPa) (Longitudinal)	Transverse shrinkage (%)	Longitudinal shrinkage (%)	Unreacted carbon (vol%)
C	1200°C, 4 h	67	3.17 ± 1.17	1.69 ± 0.37	4.3	34	0
	1400°C, 4 h	65	4.64 ± 2.10	4.34 ± 1.27	4.3	25	0
	1450°C, 4 h	64	4.41 ± 1.42	3.29 ± 0.87	3.9	21	0
	1450°C, 8 h	62	9.13 ± 1.59	4.97 ± 0.58	3	16	0
	1450°C, 15 h	60	8.67 ± 2.20	5.67 ± 0.61	2.6	16	0
	1500°C, 4 h	56	11.33 ± 2.52	4.1 ± 1.21	−5	19	0
D	1400°C, 4 h	77*	1.82 ± 0.10	0.4 ± 0.10	0	17	6
	1500°C, 4 h	73	6.77 ± 0.85	2.09 ± 0.72	−5.9	5	0
	1450°C, 4 h	75*	3.27 ± 1.91	0.58 ± 0.24	−1.5	9	5
E	1400°C, 4 h	82.5*	0.77 ± 0.16	0.47 ± 0.03	−6.2	14	13
	1450°C, 4 h	81*	3.27 ± 2.26	0.93 ± 0.84	−7.4	5	10
	1500°C, 4 h	68*	Could not test		−14	−1	11

*Porosity was corrected for unreacted carbon.

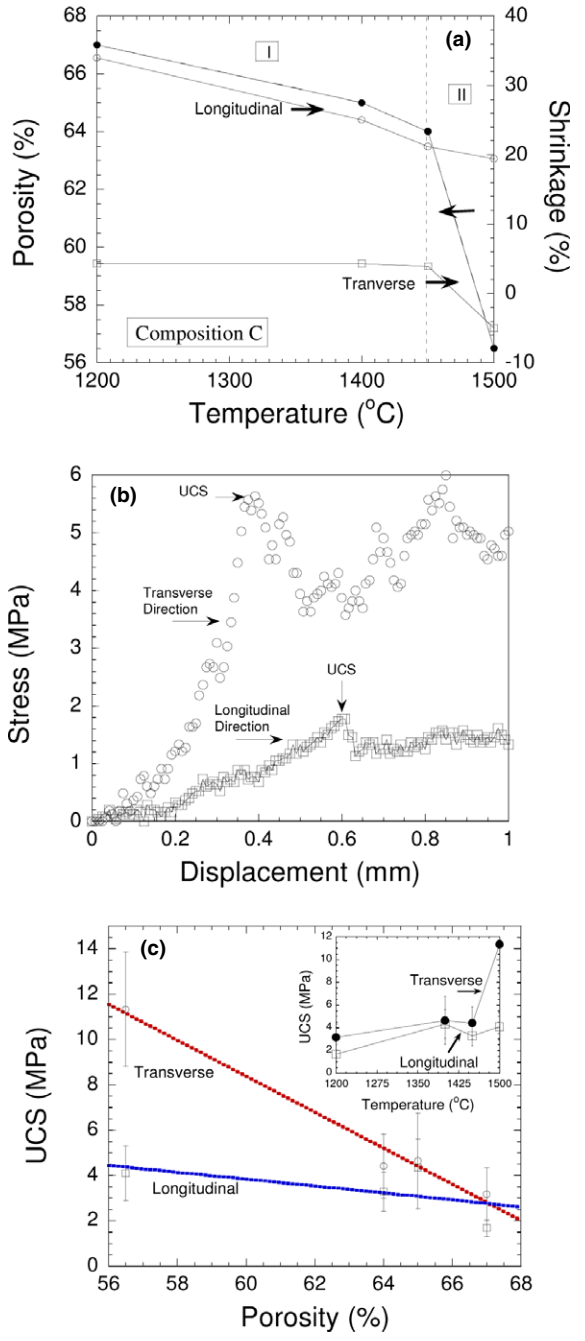

Fig. 2. Comparison of (a) porosity versus shrinkage (longitudinal and transverse) after heat treatment of composition C (Table II) at different temperatures for 4 h, (b) typical stress versus displacement plot of composition C after heat treatment at 1450°C for 4 h, and (c) variation in compressive strength (UCS) with porosity of composition C with temperature in transverse and longitudinal directions (inset shows the variation in UCS with temperature).

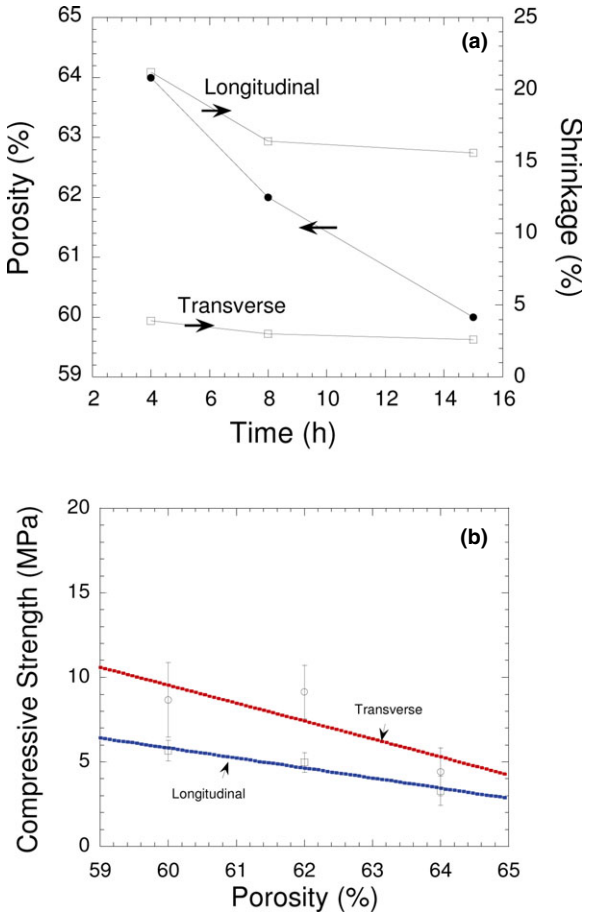

Fig. 3. Comparison of (a) porosity and shrinkage (longitudinal and transverse) and (b) variation in compressive strength with porosity in transverse and longitudinal directions as a function of time after heat treatment at 1450°C for Composition C (Table II).

pellets before and after the heat treatment process. The total volume fraction of the pore formers (V_{fp}) were also calculated from the measured weight and density of raw materials (Table II). The porosity (P) of the reacted compacts was calculated from the ratio of ρ_{RBD} and theoretical density of the oxide. In most cases, the oxide formed was rutile (4.23 g/cm^3). In a few cases, entrapped carbon was also calculated in the reacted mixture from stoichiometric calculations. In those cases, the theoretical density also incorporated the presence of entrapped carbon in the rutile matrix.

XRD patterns were collected from 10 to 90° (2θ) with a 0.02° step size and 1 second count time on a Rigaku Ultima IV X-Ray Diffractometer (Rigaku Americas, The Woodlands, TX) with Cu-Ka radiation operated at 40 kV and 44 mA. Crystalline phases were identified by

computer search-match procedures, which employ the ICDD Powder Diffraction File, using MDI Jade 9.0 Software (Materials Data, Livermore, CA).

The compressive strength of the samples was measured using a mechanical testing system (AG-IS; Shimazdu Scientific Corporation, Columbia, MD) at a deflection rate of 1 mm/min. The dimensions of the samples were ~4 mm × ~4 mm × ~4 mm cubes. The compressive strength is reported for an average of 3 samples in both transverse and longitudinal directions for all the samples. The maximum compressive strength at which a sample failed is defined as ultimate compressive strength (UCS). The dimensions of the samples were ~5 mm × ~5 mm × ~5 mm prisms. The microstructure of the Au coated samples was studied in a scanning electron microscope (SEM; Hitachi S-3400 N, Schaumburg, IL).

The sample was attached to a glass rod using hot glue and placed into a X-ray computed tomography system (MicroCT; GE, Phoenix, AZ) equipped with a 180 kV high-power nanofocus X-ray tube and a high-contrast GE DXR250RT flat panel detector. One thousand projections of the sample were acquired at a voltage of 120 kV and a current of 80 mA using a molybdenum target. Detector timing was 1000 ms and the total acquisition time was 1 hour and 6 min. Sample magnification was ×6.34 with a voxel size of ~31.6 mm. The acquired images were reconstructed into a volume data set using GE 3D computer tomography software version 2.2 (GE Sensing & Inspection Technologies GmbH, Wunstorf, Germany). The reconstructed volume was then viewed and manipulated using VGStudio Max using Volume Graphics (Volume Graphics, Charlotte, NC).

Results and Discussion

Figure 1 shows the schematics of the OIS manufacturing process. During this method, two types of pore formers were used with Ti metal powders: (i) polyethylene (PE) (pore former 1) which oxidizes and vaporizes at low temperature (<350°C) and (ii) graphite (pore former 2) which oxidizes at high temperature (>800°C). All the prepared green bodies were continuously heated at 4°C/min to the final temperature between 1400 and 1450°C in a tube furnace in air for 4 h (Table III). During the manufacturing process, porous metals compacts were completely oxidized and converted into porous oxide ceramics. The total manufacturing time during the OIS process was ~10 h.

Comparatively, the manufacturing of porous TiO_2 scaffolds of similar densities by slurry casting was tedious. The samples were fabricated by slowly heating them to 450°C at a heating rate of 0.5°C/min. After 1 h holding time at 450°C, temperature was raised to 1500°C at a rate of 3°C/min, and finally, the sintering time at this temperature was set to 40 h.[8] The total manufacturing time during a conventional process was ~66 h.

Figure 2a shows the variation in porosity and dimensional shrinkage of composition C (Table II) during heat treatment for 4 h at different temperatures. The longitudinal and transverse shrinkages changed gradually with temperature until 1450°C. However, after heat treatment at further higher temperatures, the samples showed a sharp increase in transverse shrinkage, and the

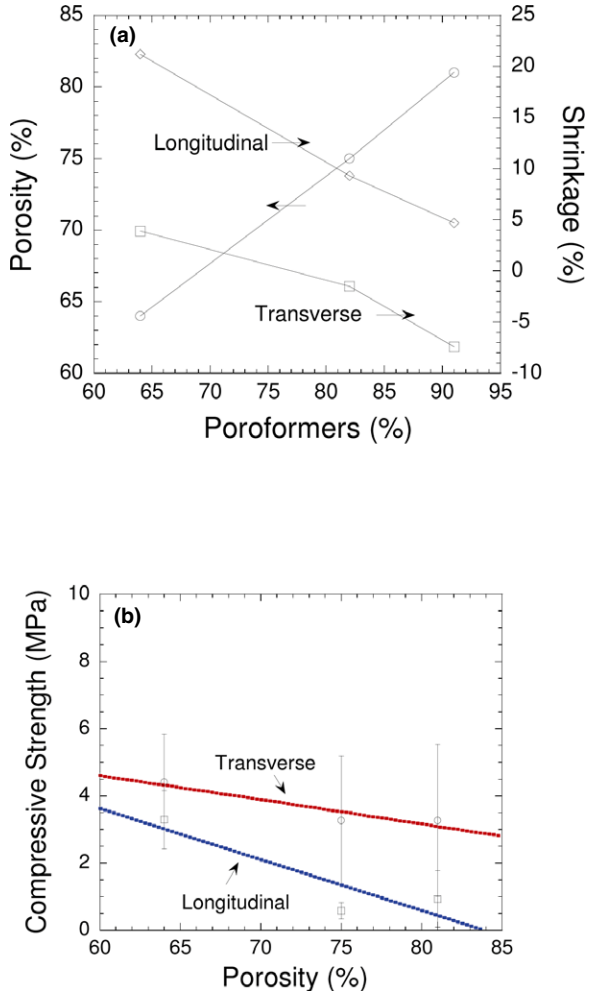

Fig. 4. Comparison of (a) porosity and shrinkage (longitudinal and transverse) as a function of different volume concentration (V_{fp}) of pore formers after heat treatment at 1450°C for 4 h and (b) variation in compressive strength with calculated porosity (P) in transverse and longitudinal directions (compositions C, D, and E – Table II).

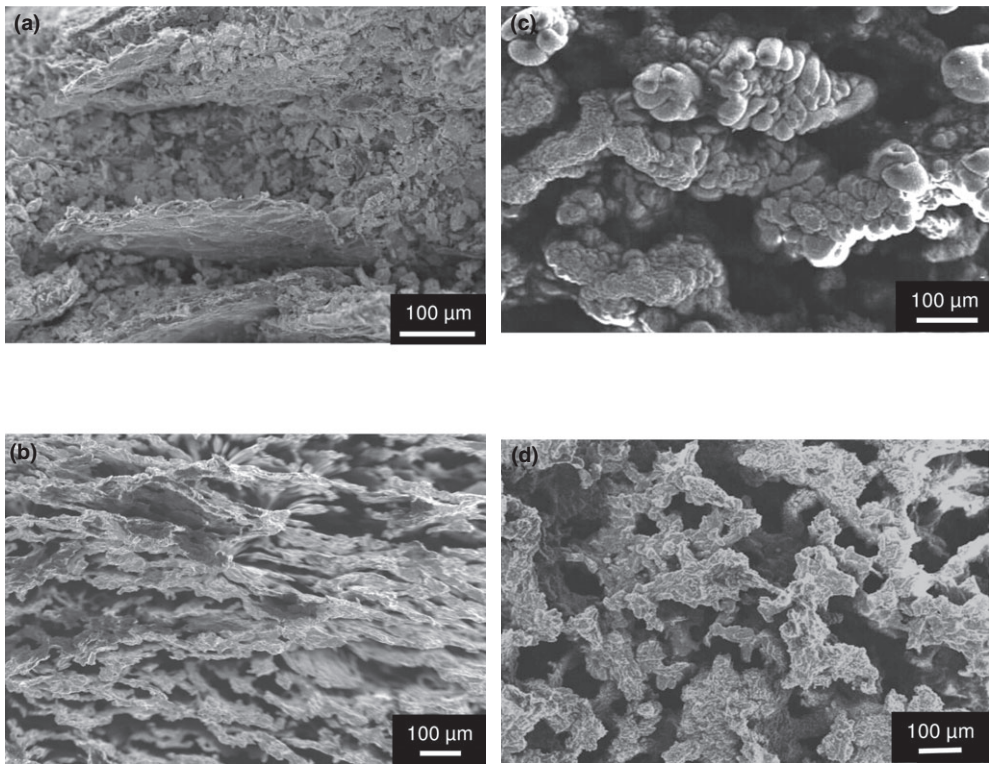

Fig. 5. SEM micrographs of (a) fractured surface of the cross section of the green body of Composition C (Table II), (b) fractured surface of the cross section of Composition C, (c) fractured surface of the cross section of Composition E (Table II), and (d) top surface of the composition E after heat treatment at 1450°C for 4 h.

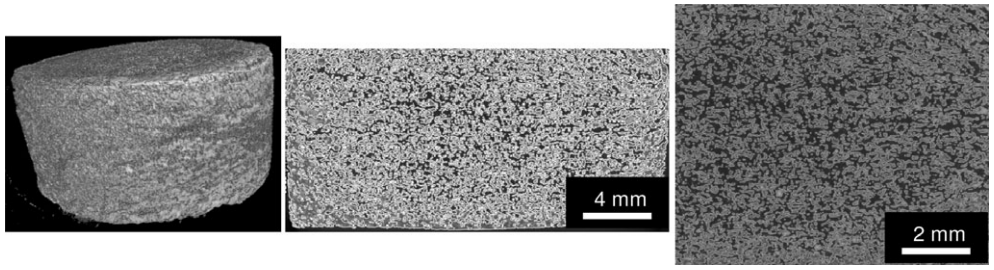

Fig. 6. Different views of composition E heat-treated at 1450°C for 4 h by X-ray tomography: (a) 3D view, 2D view of a cross section at (b) lower and (b) higher magnification.

porosity decreased concomitantly from ~64% to ~56%. Figure 2b shows a plot of compressive stress versus displacement in transverse and longitudinal directions for composition C. The samples are stronger in transverse direction as compared to longitudinal direction. Similar behavior was observed for all samples treated at different temperatures (Fig. 2c). For comparison, the inset of Fig. 2c shows the variation in UCS with temperature. The transverse UCS showed a sharper increase at 1500°C as compared to longitudinal UCS. This observation is also consistent with shrinkage measurements (Fig. 2a). This study also demonstrates that during the OIS method, the samples undergo sharp dimensional change after 1450°C. For fabricating a highly porous structures, rapid dimensional change during sintering can cause pores collapse.

Figure 3a shows variation in porosity and shrinkage as a function of time for composition C after heat treatment at 1450°C for different time intervals. Initially, the porosity decreased sharply until ~4 h; thereafter, it gradually with decreased with time. Figure 3b shows the effect of porosity on UCS. As observed earlier, the trans-

verse strength was greater than longitudinal strength, and UCS increased linearly with decrease in porosity. From these studies, we can conclude that the final sintering temperature of 1450°C for 4 h gives the optimum results.

Table III summarizes the effect of temperature and time profile on compositions with higher concentrations of pore formers (Compositions D and E, Table II). Figure 4a shows the effect of pore formers on the porosity of the sintered sample after heat treatment at 1450°C for 4 h. Clearly, as the amount of pore formers was increased in the compact, the shrinkages of the compact also increased in both transverse and longitudinal directions. However, due to the usage of higher amount of pore formers in both compositions D and E (Table II), the overall porosity of the samples also increased (Fig. 4a). Like earlier studies, the UCS in both transverse and longitudinal directions changed linearly with porosity. In addition, the UCS in transverse direction was also higher than the longitudinal direction. For example, an 81% porous sample had a transverse and longitudinal compressive strength of 3.27 ± 2.26 MPa and 0.93 ± 0.84 MPa, respectively. Comparatively, Tiainen *et al.*[8] had observed a compressive strength of 1.5–2 MPa in 82% porous TiO_2 scaffolds manufactured at 1500°C using the ceramic slurry method outlined in the earlier section. Thus, we can conclude that OIS manufacturing method can produce porous oxide ceramics of comparable strength and porosity as conventional methods using a lower manufacturing temperature and faster heating cycles.

The final temperature of sintering also played a very important role in sintering. The samples heat-treated at 1400°C for 4 h had lower compressive strength as compared to samples heated at 1450°C for 4 h (Table III). In addition, samples treated at 1500°C showed the highest shrinkage (Fig. 2 and Table III). For example, the composition E heat-treated at 1500°C for 4 h could not be characterized as the sample collapsed under the sintering pressure. In future, if this manufacturing method is adopted in other oxide model systems, then it is critical to balance to the sintering time and temperatures along with the pore former content in the tailored compositions.

Figure 5a shows the FESEM micrograph of the green body of composition C. In the microstructure, the graphite flakes are preferentially oriented parallel to the transverse direction can be observed. Figures 5b shows the microstructure of Composition C after oxidation at 1450°C for 4 h. After the graphite flakes are burnout, they leave behind anisotropic pores oriented parallel to the transverse direction. Due to this reason, the samples are macroporous and have a pore size (w) greater than

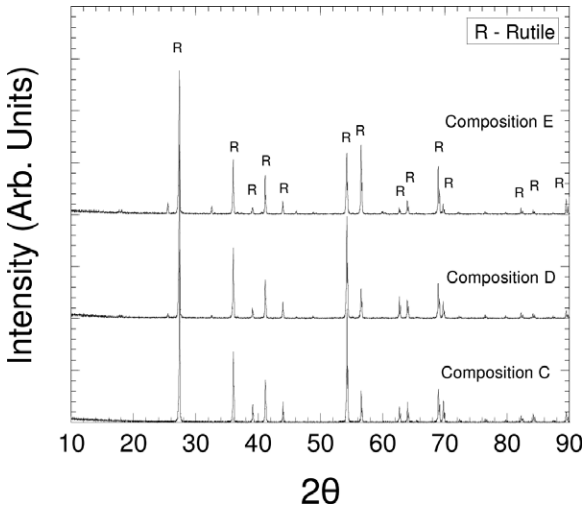

Fig. 7. XRD of compositions C, D, and E after oxidation at 1450°C for 4 h (Table II).

100 μm. Similarly, Fig. 5c shows anisotropic macropores are oriented parallel to the transverse direction in composition E (Table II), whereas on the top surface, the pores are randomly distributed (Fig. 5d). These micrographs also clearly show that the solid network is interconnected. This observation was also confirmed by X-ray microtomography of the composition E (Fig. 6). By inspecting the Figs. 6b–c, we can conclude that pores are interconnected and are aligned parallel to the transverse direction. The anisotropic microstructure can explain the higher strength in transverse direction as compared to the longitudinal direction. It is further argued that using uniform sized pore formers, it will be possible to form highly porous isotropic microstructures using OIS method.

XRD shows that all the oxides formed are predominantly rutile (Fig. 7). The compositions D and E had entrapped residual carbon particles (Table III). More detailed studies are needed to understand the nature of Carbon particles and its effect on conductivity of these porous scaffolds.

Conclusions

The authors have developed a simpler and faster method of manufacturing porous ceramics by converting porous metal compacts into macroporous oxide samples by oxidizing them at optimum temperatures. Using the novel method, it is also possible to manufacture porous solids over a wide range of porosity. The microstructure of these solids is anisotropic due to the use of flaky graphite particles as pore formers. The compression

strength of the porous solids produced by this method is comparable, if not better than the porous solids produced by conventional methods.

Acknowledgments

One of the author (SG) would like to acknowledge University of North Dakota Start Up and Seed Grant for the financial support. NDSU Electron Microscopy Center core facility is acknowledged for the microscopy and X-ray tomography studies. This material is based upon work supported by the National Science Foundation under Grant No. 0619098, and 1229417. Any opinions, findings, and conclusions or recommendations expressed in this material are those of the author(s) and do not necessarily reflect the views of the National Science Foundation.

References

1. J. Luyten, S. Mullens, J. Cooymans, A. M. De Wilde, I. Thijs, and R. Kemps, *J. Eur. Ceram. Soc.*, 29 829–832 (2009).
2. P. Colombo, *Phil. Trans. R. Soc. A*, 364 109–124 (2006).
3. L. J. Gibson and M. F. Ashby, *Cellular Solids – Structure and Properties*, 2nd edition, Cambridge Solid State Science Series, Cambridge University Press, Cambridge, 1997.
4. J. E. Reed, *Principles of Ceramic Processing*, 2nd edition, John Wiley and Sons, New York, NY, 1995.
5. K. Nakata, M. Sakai, T. Ochiai, T. Murakami, K. Takagi, and A. Fujishima, *Mat. Letts.*, 70 160–162 (2012).
6. L. Ren, Y. Zeng, and D. Jiang, *Ceram. Int.*, 35 1267–1270 (2009).
7. T. Ohji and M. Fukushima, *Int. Mater. Rev.*, 57 [2] 115–131 (2012).
8. H. Tiainen, S. P. Lyngstadaas, J. Ei Ellingsen, and H. J. Haugen, *J. Mater. Sci. Mater. Med.*, 21 2783–2792 (2010)
9. J. H. She, Z. Y. Deng, J. Daniel-Doni, and T. Ohji, *J. Mater. Sci.*, 37 3615–3622 (2002).
10. J. She, J.-F. Yang, N. Kondo, T. Ohji, S. Kanzaki, and Z.-Y. Deng, *J. Am. Ceram. Soc.*, 85 2852–2854 (2002).
11. J. H. She, T. Ohji, and S. Kanzaki, *J. Eur. Ceram. Soc.*, 24, 331–334 (2003).
12. S. Gupta, U.S. Patent Application, 2013.

REFERENCES

[1] J. C. Hower, "Petrographic examination of coal-combustion fly ash," *International Journal of Coal Geology*, vol. 92, pp. 90-97, 2012.

[2] K. Styszko-Grochowiak, J. Gołaś, H. Jankowski, and S. Koziński, "Characterization of the coal fly ash for the purpose of improvement of industrial on-line measurement of unburned carbon content," *Fuel*, vol. 83, pp. 1847-1853, 2004.

[3] (2011). *World Coal Association, Coal statistics*. Available: http://www.worldcoal.org/resources/ coal-statistics/

[4] (2011). *American Coal Ash Association. Revised 2009 Coal Combustion Product (CCP) Production & Use Survey Report*. Available: http://www.acaa-usa.org/associations/8003/ files/2009_Production_and_Use_Survey_Revised_100511.pdf

[5] S. Wang, "Application of Solid Ash Based Catalysts in Heterogeneous Catalysis," *Environmental Science & Technology*, vol. 42, pp. 7055-7063, 2008.

[6] M. Ahmaruzzaman, "A review on the utilization of fly ash," *Progress in Energy and Combustion Science*, vol. 36, pp. 327-363, 2010.

[7] A. B. Mukherjee, R. Zevenhoven, P. Bhattacharya, K. S. Sajwan, and R. Kikuchi, "Mercury flow via coal and coal utilization by-products: A global perspective," *Resources, Conservation and Recycling*, vol. 52, pp. 571-591, 2008.

[8] K. J. Reddy, S. John, H. Weber, M. D. Argyle, P. Bhattacharyya, D. T. Taylor, *et al.*, "Simultaneous capture and mineralization of coal combustion flue gas carbon dioxide (CO2)," *Energy Procedia*, vol. 4, pp. 1574-1583, 2011.

[9] R. S. Blissett and N. A. Rowson, "A review of the multi-component utilisation of coal fly ash," *Fuel*, vol. 97, pp. 1-23, 2012.

[10] B. Lothenbach, K. Scrivener, and R. D. Hooton, "Supplementary cementitious materials," *Cement and Concrete Research*, vol. 41, pp. 1244-1256, 2011.

[11] M. J. McCarthy and R. K. Dhir, "Towards maximising the use of fly ash as a binder," *Fuel*, vol. 78, pp. 121-132, 1999.

[12] P. Duxson, A. Fernández-Jiménez, J. L. Provis, G. C. Lukey, A. Palomo, and J. S. J. v. Deventer, "Geopolymer technology: the current state of the art," *Journal of Materials Science*, vol. 42, pp. 2917-2933, 2007.

[13] P. Duxson, J. L. Provis, G. C. Lukey, and J. S. J. van Deventer, "The role of inorganic polymer technology in the development of 'green concrete'," *Cement and Concrete Research*, vol. 37, pp. 1590-1597, 2007.

[14] A. Fernández-Jiménez and A. Palomo, "Characterisation of fly ashes. Potential reactivity as alkaline cements☆," *Fuel*, vol. 82, pp. 2259-2265, 2003.

[15] A. Fernández-Jiménez and A. Palomo, "Composition and microstructure of alkali activated fly ash binder: Effect of the activator," *Cement and Concrete Research*, vol. 35, pp. 1984-1992, 2005.

[16] X. Guo, H. Shi, L. Chen, and W. A. Dick, "Alkali-activated complex binders from class C fly ash and Ca-containing admixtures," *Journal of Hazardous Materials,* vol. 173, pp. 480-486, 2010.
[17] X. Guo, H. Shi, and W. A. Dick, "Compressive strength and microstructural characteristics of class C fly ash geopolymer," *Cement and Concrete Composites,* vol. 32, pp. 142-147, 2010.
[18] A. Palomo, M. W. Grutzeck, and M. T. Blanco, "Alkali-activated fly ashes: A cement for the future," *Cement and Concrete Research,* vol. 29, pp. 1323-1329, 1999.
[19] G. S. Ryu, Y. B. Lee, K. T. Koh, and Y. S. Chung, "The mechanical properties of fly ash-based geopolymer concrete with alkaline activators," *Construction and Building Materials,* vol. 47, pp. 409-418, 2013.
[20] K. Somna, C. Jaturapitakkul, P. Kajitvichyanukul, and P. Chindaprasirt, "NaOH-activated ground fly ash geopolymer cured at ambient temperature," *Fuel,* vol. 90, pp. 2118-2124, 2011.
[21] S. Gupta and M. F. Riyad, "Low-Alkali Fly Ash Cement and Method of Making," 2013.
[22] F. Massazza, "Structures and performance of cements," *University of Sheffield, England,* 2003.
[23] J. G. S. Van Jaarsveld, J. S. J. Van Deventer, and L. Lorenzen, "The potential use of geopolymeric materials to immobilise toxic metals: Part I. Theory and applications," *Minerals Engineering,* vol. 10, pp. 659-669, 1997.
[24] T. Bakharev, "Thermal behaviour of geopolymers prepared using class F fly ash and elevated temperature curing," *Cement and Concrete Research,* vol. 36, pp. 1134-1147, 2006.
[25] D. Krizan and B. Zivanovic, "Effects of dosage and modulus of water glass on early hydration of alkali–slag cements," *Cement and Concrete Research,* vol. 32, pp. 1181-1188, 2002.
[26] F. Pacheco-Torgal, J. Castro-Gomes, and S. Jalali, "Alkali-activated binders: A review: Part 1. Historical background, terminology, reaction mechanisms and hydration products," *Construction and Building Materials,* vol. 22, pp. 1305-1314, 2008.
[27] T. Bakharev, "Geopolymeric materials prepared using Class F fly ash and elevated temperature curing," *Cement and Concrete Research,* vol. 35, pp. 1224-1232, 2005.
[28] J. C. Swanepoel and C. A. Strydom, "Utilisation of fly ash in a geopolymeric material," *Applied Geochemistry,* vol. 17, pp. 1143-1148, 2002.
[29] P. Chindaprasirt, T. Chareerat, and V. Sirivivatnanon, "Workability and strength of coarse high calcium fly ash geopolymer," *Cement and Concrete Composites,* vol. 29, pp. 224-229, 2007.
[30] D. Panias, I. P. Giannopoulou, and T. Perraki, "Effect of synthesis parameters on the mechanical properties of fly ash-based geopolymers," *Colloids and Surfaces A: Physicochemical and Engineering Aspects,* vol. 301, pp. 246-254, 2007.
[31] N. Bouzoubaâ, M. Zhang, and V. Malhotra, "Effects of grinding on physical & mechanical properties of high-volume fly ash blended cements," *World cement,* vol. 29, pp. 96-101, 1998.
[32] S. Huang and J. Cheng, "Kinetic of reaction in the system fly ash-Ca (OH) 2-H2O," *Journal of Chinese Ceramic Society,* vol. 14, pp. 191-197, 1986.

[33] S. K. Antiohos, A. Papageorgiou, V. G. Papadakis, and S. Tsimas, "Influence of quicklime addition on the mechanical properties and hydration degree of blended cements containing different fly ashes," *Construction and Building Materials,* vol. 22, pp. 1191-1200, 2008.
[34] J. Temuujin, R. P. Williams, and A. van Riessen, "Effect of mechanical activation of fly ash on the properties of geopolymer cured at ambient temperature," *Journal of Materials Processing Technology,* vol. 209, pp. 5276-5280, 2009.
[35] Z. Li and S. Liu, "Influence of slag as additive on compressive strength of fly ash-based geopolymer," *Journal of materials in civil engineering,* vol. 19, pp. 470-474, 2007.
[36] D. H. Gray and Y.-K. Lin, "Engineering Properties of Compacted Fly Ash," *Journal of the Soil Mechanics and Foundations Division,* vol. 98, pp. 361-380, 1972.
[37] S. Antiohos and S. Tsimas, "Activation of fly ash cementitious systems in the presence of quicklime: Part I. Compressive strength and pozzolanic reaction rate," *Cement and Concrete Research,* vol. 34, pp. 769-779, 2004.
[38] W. Ma and P. W. Brown, "Hydrothermal reactions of fly ash with Ca(OH)2 and CaSO4·2H2O," *Cement and Concrete Research,* vol. 27, pp. 1237-1248, 1997.
[39] W. Ma, C. Liu, P. W. Brown, and S. Komarneni, "Pore structures of fly ashes activated by Ca(OH)2 and CaSO4 · 2H2O," *Cement and Concrete Research,* vol. 25, pp. 417-425, 1995.
[40] C. Shi, "Studies on Several Factors Affecting Hydration and Properties of Lime-Pozzolan Cements," *Journal of Materials in Civil Engineering,* vol. 13, pp. 441-445, 2001.
[41] D. J. Fauth, Y. Soong, and C. M. White, "Carbon sequestration utilizing industrial solid residues," in *Preprints Symposium*, 2002, pp. 37-38.
[42] M. Back, M. Kuehn, H. Stanjek, and S. Peiffer, "Reactivity of alkaline lignite fly ashes towards CO2 in water," *Environmental science & technology,* vol. 42, pp. 4520-4526, 2008.
[43] G. Montes-Hernandez, R. Pérez-López, F. Renard, J. M. Nieto, and L. Charlet, "Mineral sequestration of CO2 by aqueous carbonation of coal combustion fly-ash," *Journal of Hazardous Materials,* vol. 161, pp. 1347-1354, 2009.
[44] G. W. M. Muriithi Grace Nyambura, "Carbonation of brine impacted fractionated coal fly ash: implications for CO2 sequestration," *Journal of environmental management,* vol. 92, pp. 655-64, 2010.
[45] B. H. H. R. M. Dilmore, "Sequestration of CO2 in Mixtures of Caustic Byproduct and Saline Waste Water," *Environmental Engineering Science - ENVIRON ENG SCI*, 2009.
[46] J. A. Schramke, "Neutralization of alkaline coal fly ash leachates by CO2(g)," *Applied Geochemistry,* vol. 7, pp. 481-492, 1992.
[47] Y. Soong, D. L. Fauth, B. H. Howard, J. R. Jones, D. K. Harrison, A. L. Goodman, *et al.*, "CO2 sequestration with brine solution and fly ashes," *Energy Conversion and Management,* vol. 47, pp. 1676-1685, 2006.
[48] K. J. R. T. A. Tawfic, "Reaction of CO2 with clean coal technology ash to reduce trace element mobility," vol. 84, pp. 385-398, 1995.
[49] A. Uliasz-Bocheńczyk, E. Mokrzycki, Z. Piotrowski, and R. Pomykała, "Estimation of CO2 sequestration potential via mineral carbonation in fly ash from lignite combustion in Poland," *Energy Procedia,* vol. 1, pp. 4873-4879, 2009.

[50] M. L. Gray, Y. Soong, K. J. Champagne, J. Baltrus, R. W. Stevens Jr, P. Toochinda, *et al.*, "CO2 capture by amine-enriched fly ash carbon sorbents," *Separation and Purification Technology*, vol. 35, pp. 31-36, 2004.
[51] I. Majchrzak-Kucęba and W. Nowak, "Development of Fly Ash-Based Sorbent to Capture CO2 from Flue Gas," in *Proceedings of the 20th International Conference on Fluidized Bed Combustion*, G. Yue, H. Zhang, C. Zhao, and Z. Luo, Eds., ed: Springer Berlin Heidelberg, 2010, pp. 596-602.
[52] M. Olivares-Marín, T. C. Drage, and M. M. Maroto-Valer, "Novel lithium-based sorbents from fly ashes for CO2 capture at high temperatures," *International Journal of Greenhouse Gas Control*, vol. 4, pp. 623-629, 2010.
[53] J.-H. Wee, "A review on carbon dioxide capture and storage technology using coal fly ash," *Applied Energy*, vol. 106, pp. 143-151, 2013.
[54] S. Sahoo, M. Ö. Seydibeyoğlu, A. K. Mohanty, and M. Misra, "Characterization of industrial lignins for their utilization in future value added applications," *Biomass and Bioenergy*, vol. 35, pp. 4230-4237, 2011.
[55] X. Pan, X. Zhang, D. J. Gregg, and J. N. Saddler, "Enhanced enzymatic hydrolysis of steam-exploded douglas fir wood by alkali-oxygen post-treatment," *Applied Biochemistry and Biotechnology*, vol. 115, pp. 1103-1114, 2004.
[56] R. Singh, S. Singh, K. D. Trimukhe, K. V. Pandare, K. B. Bastawade, D. V. Gokhale, *et al.*, "Lignin–carbohydrate complexes from sugarcane bagasse: Preparation, purification, and characterization," *Carbohydrate Polymers*, vol. 62, pp. 57-66, 2005.
[57] D. Schorr, P. N. Diouf, and T. Stevanovic, "Evaluation of industrial lignins for biocomposites production," *Industrial Crops and Products*, vol. 52, pp. 65-73, 2014.
[58] G. W. G, H. S. U. O. H.-H, R. D. L, F. R. C, and W. U. L. C.-F, "Lignin-Derived Polyols, Polyisocyanates, and Polyurethanes," in *Urethane Chemistry and Applications*. vol. 172, ed: AMERICAN CHEMICAL SOCIETY, 1981, pp. 311-338.
[59] A. De Chirico, M. Armanini, P. Chini, G. Cioccolo, F. Provasoli, and G. Audisio, "Flame retardants for polypropylene based on lignin," *Polymer Degradation and Stability*, vol. 79, pp. 139-145, 2003.
[60] A. De Chirico, G. Audisio, F. Provasoli, A. G. Schieroni, B. Focher, and B. Grossi, "Differential scanning calorimetry and thermal gravimetric analysis of lignin blended with triglycidyl isocyanurate," *Die Angewandte Makromolekulare Chemie*, vol. 228, pp. 51-58, 1995.
[61] G. Gallina, E. Bravin, C. Badalucco, G. Audisio, M. Armanini, A. De Chirico, *et al.*, "Application of cone calorimeter for the assessment of class of flame retardants for polypropylene," *Fire and Materials*, vol. 22, pp. 15-18, 1998.
[62] M. Canetti, A. De Chirico, and G. Audisio, "Morphology, crystallization and melting properties of isotactic polypropylene blended with lignin," *Journal of Applied Polymer Science*, vol. 91, pp. 1435-1442, 2004.
[63] J. F. Kadla and S. Kubo, "Miscibility and Hydrogen Bonding in Blends of Poly(ethylene oxide) and Kraft Lignin," *Macromolecules*, vol. 36, pp. 7803-7811, 2003.
[64] J. F. Kadla and S. Kubo, "Lignin-based polymer blends: analysis of intermolecular interactions in lignin–synthetic polymer blends," *Composites Part A: Applied Science and Manufacturing*, vol. 35, pp. 395-400, 2004.

[65] S. Kubo and J. F. Kadla, "Kraft lignin/poly(ethylene oxide) blends: Effect of lignin structure on miscibility and hydrogen bonding," *Journal of Applied Polymer Science,* vol. 98, pp. 1437-1444, 2005.
[66] K. Weihua, Y. He, N. Asakawa, and Y. Inoue, "Effect of lignin particles as a nucleating agent on crystallization of poly(3-hydroxybutyrate)," *Journal of Applied Polymer Science,* vol. 94, pp. 2466-2474, 2004.
[67] W. Thielemans, E. Can, S. S. Morye, and R. P. Wool, "Novel applications of lignin in composite materials," *Journal of Applied Polymer Science,* vol. 83, pp. 323-331, 2002.
[68] A. Y. Kharade and D. D. Kale, "Lignin-filled polyolefins," *Journal of Applied Polymer Science,* vol. 72, pp. 1321-1326, 1999.
[69] J. H. Lora and W. G. Glasser, "Recent Industrial Applications of Lignin: A Sustainable Alternative to Nonrenewable Materials," *Journal of Polymers and the Environment,* vol. 10, pp. 39-48, 2002.
[70] A. Duval and M. Lawoko, "A review on lignin-based polymeric, micro- and nano-structured materials," *Reactive and Functional Polymers*.
[71] G. Toriz, F. Denes, and R. A. Young, "Lignin-polypropylene composites. Part 1: Composites from unmodified lignin and polypropylene," *Polymer Composites,* vol. 23, pp. 806-813, 2002.
[72] P. Alexy, B. Košíková, and G. Podstránska, "The effect of blending lignin with polyethylene and polypropylene on physical properties," *Polymer,* vol. 41, pp. 4901-4908, 2000.
[73] X. Chen, S. Wu, and J. Zhou, "Influence of porosity on compressive and tensile strength of cement mortar," *Construction and Building Materials,* vol. 40, pp. 869-874, 2013.
[74] C. Freidin, "Cementless pressed blocks from waste products of coal-firing power station," *Construction and Building Materials,* vol. 21, pp. 12-18, 2007.
[75] D. P. H. Hasselman, "Griffith Flaws and the Effect of Porosity on Tensile Strength of Brittle Ceramics," *Journal of the American Ceramic Society,* vol. 52, pp. 457-457, 1969.
[76] J. S. Reed, *Principles of Ceramics Processing,* Second ed.: John Wiley and Sons, Inc., 1995.
[77] M. Röβler and I. Odler, "Investigations on the relationship between porosity, structure and strength of hydrated portland cement pastes I. Effect of porosity," *Cement and Concrete Research,* vol. 15, pp. 320-330, 1985.
[78] E. Ryshkewitch, "Compression Strength of Porous Sintered Alumina and Zirconia," *Journal of the American Ceramic Society,* vol. 36, pp. 65-68, 1953.
[79] V. Živica and M. Križma, "Dependence of efficiency of pressure compaction on the cement type used," *Construction and Building Materials,* vol. 25, pp. 3073-3077, 2011.
[80] R. Gabrovšek, T. Vuk, and V. e. Kaučič, "Evaluation of the hydration of Portland cement containing various carbonates by means of thermal analysis," *Acta chimica slovenica,* vol. 53, pp. 159-165, 2006.
[81] V. Živica, "Effects of the very low water/cement ratio," *Construction and Building Materials,* vol. 23, pp. 3579-3582, 2009.
[82] T. Gatta, E. Gregori, F. Marini, M. Tomassetti, G. Visco, and L. Campanella, "New approach to the differentiation of marble samples using thermal analysis and chemometrics in order to identify provenance," *Chemistry Central Journal,* vol. 8, p. 35, 2014.

[83] Z. Ioannou, L. Zoumpoulakis, I. Halikia, and T. Teloniati, "Overall kinetic study of non-isothermal decomposition of calcium carbonate," *Mineral Processing and Extractive Metallurgy*, vol. 118, pp. 98-104, 2009.
[84] N. Saikia, P. Sengupta, P. K. Gogoi, and P. C. Borthakur, "Kinetics of dehydroxylation of kaolin in presence of oil field effluent treatment plant sludge," *Applied clay science*, vol. 22, pp. 93-102, 2002.
[85] J. Davidovits, "Synthetic mineral polymer compound of the silicoaluminates family and preparation process," ed: Google Patents, 1984.
[86] J. Xie and O. Kayali, "Effect of initial water content and curing moisture conditions on the development of fly ash-based geopolymers in heat and ambient temperature," *Construction and Building Materials*, vol. 67, Part A, pp. 20-28, 2014.
[87] P. Rovnaník, "Effect of curing temperature on the development of hard structure of metakaolin-based geopolymer," *Construction and Building Materials*, vol. 24, pp. 1176-1183, 2010.
[88] P. W. Brown, "The System Na2O-CaO-SiO2-H2O," *Journal of the American Ceramic Society*, vol. 73, pp. 3457-3461, 1990.
[89] R. O. Lokken, J. W. Shade, and P. F. Martin, "Effect of curing temperature on the properties of cementitious waste forms," in *MRS Proceedings*, 1989, p. 23.
[90] N. Pandian and S. Balasubramonian, "Permeability and consolidation behavior of fly ashes," *Journal of testing and evaluation*, vol. 27, pp. 337-342, 1999.
[91] E. U. Haq, S. K. Padmanabhan, and A. Licciulli, "In-situ carbonation of alkali activated fly ash geopolymer," *Construction and Building Materials*, vol. 66, pp. 781-786, 2014.
[92] M. F. Bertos, X. Li, S. Simons, C. Hills, and P. Carey, "Investigation of accelerated carbonation for the stabilisation of MSW incinerator ashes and the sequestration of CO 2," *Green Chemistry*, vol. 6, pp. 428-436, 2004.
[93] R. Perez-Lopez, G. Montes-Hernandez, J. Nieto, F. Renard, and L. Charlet, "Carbonation of alkaline paper mill waste to reduce CO_2 greenhouse gas emissions into the atmosphere," *Applied Geochemistry*, vol. 23, pp. 2292-2300, 2008.